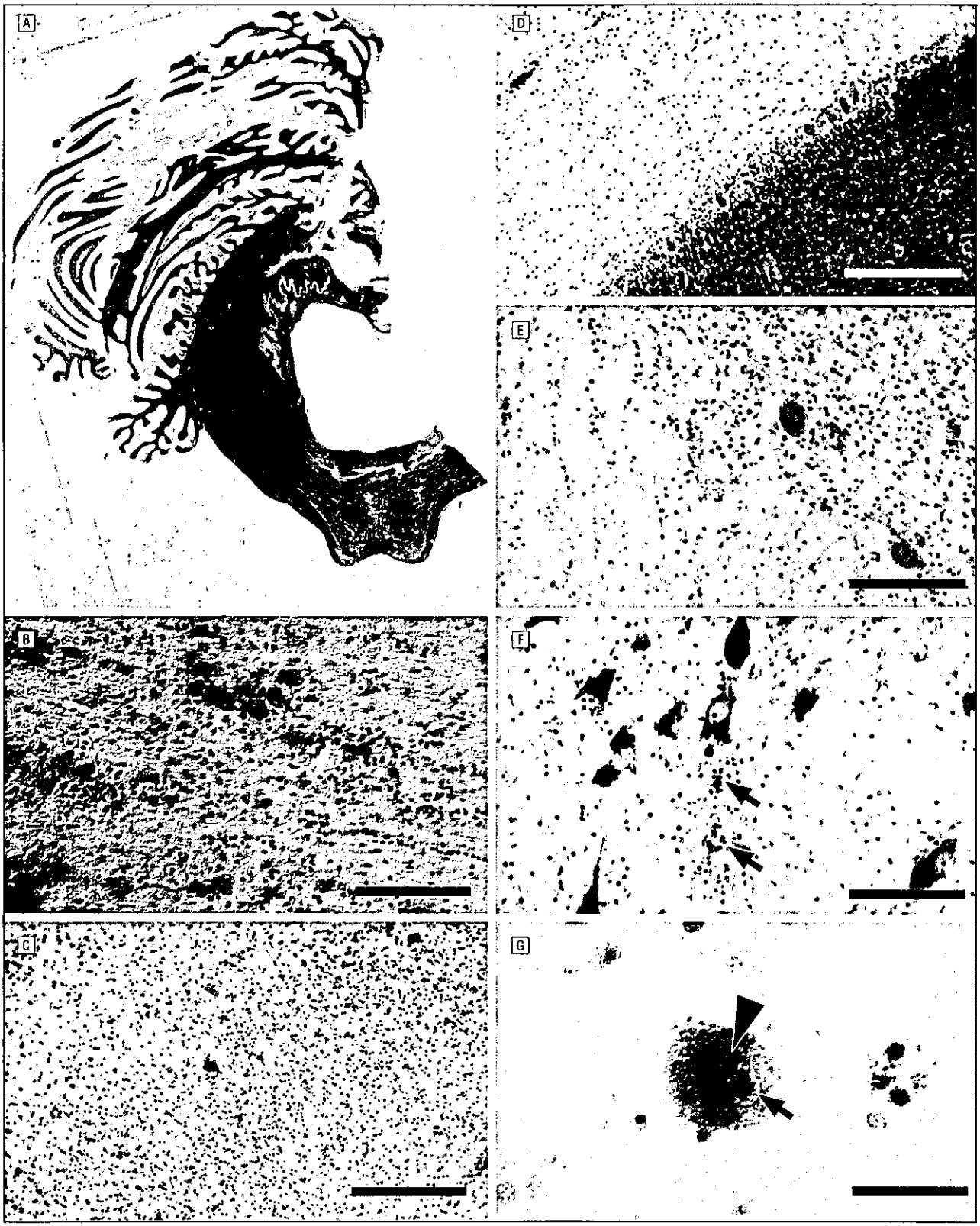

Figure 3. Present-day photographs of original slides. Macroscopic and microscopic findings in the cerebellum and basal ganglia. A, Pons and cerebellum. Despite the atrophy in the pontine base and dentate nucleus, the cerebellar cortex is relatively well preserved (myelin). B, Pontine nuclei. Gliosis and degeneration of pontine neurons (Nissl; scale bar, 50 μm). C, Dentate nucleus. Neuronal depletion and gliosis (Nissl; scale bar, 200 μm). D, Cerebellar Purkinje cells are well preserved (hematoxylin-eosin; scale bar, 200 μm) E, Oculomotor nucleus. Massive gliosis and neuronal depletion (Nissl; scale bar, 50 μm). F, Substantia nigra (pars compacta). Gliosis and free-melanin pigments (arrows) (Nissl; scale bar, 50 μm). G, Pallidum. A neuronal cell containing nucleolus (arrow) and an additional round structure (arrowhead) reminiscent of intranuclear inclusion (Nissl; scale bar, 20 μm).

Table 1. Similarity in Clinical Features Between Patients From the Haudebourg Family and Patients With Machado-Joseph Disease (MJD)

Clinical Feature	Patients From Haudenbourg Family	Autopsy Case	Patients With MJD
Heredity	AD compatible	AD compatible	AD
Ataxia	Present	Present	Present
Pyramidal signs	Present	Present	Present
Rigidity	Present	Present	Present
Mask-like face	*absence de mimique* (absence of facial expression)	*visage sans mimique* (expressionless face)	Present
Exophthalmos	*regard étonné* (astonished gaze); *yeux grand ouverts* (wide opened eyes)	Present	Stared gaze
EOM	Diplopia (nystagmus)	Nuclear paresis	Nuclear paresis
Vestibular dysfunction	Unknown	Disturbed	Caloric response, absent

Abbreviations: AD, autosomal dominant; EOM, extraocular movements.

MICROSCOPIC REEXAMINATION OF THE STAINED PREPARATIONS

Only several specimens embedded in celloidin are still available for neuropathological examination. In addition to the original description depicted earlier, the following lesions were identified: anterior horn (Figure 1C), Clarke column (Figure 1D), hypoglossal nucleus, oculomotor nucleus (Figure 3E), pars compacta of substantia nigra (Figure 3F), and pallidum. The inferior olivary nucleus was well preserved (Figure 2A). A Nomarski view of a neuron in the pallidum on a Nissl-stained section identified a possible nuclear inclusion (Figure 3G) reminiscent of those seen in most cytosine-adenine-guanine (CAG) triplet expansion diseases including MJD.[16-18]

COMMENT

Clinical features of this patient included ataxic gait with spasticity, appendicular ataxia, and slurred speech, which are shared with so-called spinocerebellar degenerations. Increased muscle tone and increased deep tendon reflexes, together with nuclear ophthalmoparesis, exophthalmos, and mask-like face were described in patients from the Haudebourg family (**Table 1**),[3,8-11,19] which reasonably led to the clinical diagnosis of HAC. These clinical features, however, have been described in some patients with the diagnosis of MJD (Table 1),[20] although the clinical features of MJD are highly variable.[21-24] Some of these features other than ataxia have also been described sometimes in patients with spinocerebellar ataxia type 1,[20,25] whereas vestibular disturbance of central origin is a distinctive feature of MJD.[26,27] Although stared gaze or bulging eye is a probable (but not exclusive) indicator of MJD,[20,25] *l'aspect étonné du facies* (astonished look of the face) or *les yeux grand ouverts* (wide, opened eyes) described in the affected members from the Haudebourg family[3] or exophthalmos in this autopsy case may be identical.

An association of pigmentary retinopathy to autosomal dominant cerebellar ataxia was considered to be a hallmark for autosomal dominant cerebellar ataxia II,[28,29] consistently found in spinocerebellar ataxia type 7.[30-32] Visual impairment due to optic atrophy, however, has recently been found to be not uncommon (13 [22.8%] of 57 cases) in a cohort of genetically confirmed cases of MJD.[33] Indeed, several patients from the Haudebourg family, as well as the first autopsied case reported as HAC,[34] also developed visual impairment. Although ultimate genetic abnormality has not yet been confirmed in the family of the autopsy case, the mode of inheritance was compatible with autosomal dominant inheritance, shared by most of the hereditary ataxias linked to CAG triplet expansion diseases, including MJD. Had trained clinical neurologists of today had a chance to examine the clincial findings of this case, they would have suspected that MJD was the most probable diagnosis even before genetic analysis.

Pathological description from this autopsy record stated that the lesions included the spinal cord (spinocerebellar tracts, anterolateral fascicles, and posterior column in the upper cervical segment), pontine nuclei, dentate nucleus, and the cerebellum as presented in **Table 2**. Involvement of the spinocerebellar tracts and anterolateral fascicles described in this autopsy case is among the principal features of HAC as described in autopsied patients from the Haudebourg family.[8-11] This is reminiscent of the morphological changes of the spinal cord in cases of MJD.[20-24,35,36] Severe involvement of the pontine nucleus with relative preservation of the cerebellar cortex, again noted in the patients from the Haudebourg family,[9,19] was recorded in this autopsy case, which is also characteristic of MJD.[20,21,23] Although this autopsy record only mentioned that the medulla oblongata was not atrophic, reviewing the slides confirmed that inferior olives were well preserved (Figure 2A), as reported in the patients from the Haudebourg family (Figure 2B and C, Table 2).[8-11,19] This is another distinguishing feature of MJD (Figure 2D) not observed in spinocerebellar ataxia type 1, type 2,[20] or type 7.[31] Relative preservation of the cerebellar cortex and inferior olives with preferential involvement of pontocerebellar and spinocerebellar projections, as seen in this autopsy case, are also shared with the autopsy cases from the Haudebourg family and individuals with MJD (Table 2). Because cerebellipetal systems wired through mossy fibers are preferentially affected, this combination could be grouped under the name *mossy-fiber type cerebellipetal degeneration*,[19] which may further include an autopsy case[37] from a large family[4] and spinopontine degeneration (SPD), initially reported by Boller and Seggara[38-40] (Table 2). It is worth mentioning that Boller and Seggara noted that clinicopathological features of SPD were similar to those described [41,42] in patients from the Haudebourg family with HAC.[8-11] Moreover, the similarity between SPD and MJD[36,43] was corroborated by the identification of SPD and MJD in the

Table 2. Pathological Features Shared by Patients From the Haudebourg Family and Patients With Machado-Joseph Disease (MJD) and Spinopontine Degeneration (SPD)

Pathological Feature	Patients From Haudebourg Family	Autopsy Case	Patients With MJD	Patients With SPD
Severity of atrophy*				
Spinocerebellar tracts	Moderate	Mild	Moderate	Mild
Clarke column	Moderate	Moderate	Severe	Moderate
Pyramidal tract	None	None	None	None
Anterolateral fascicle	Moderate	Mild	Severe	Mild
Anterior horn	Moderate	Mild	Severe	Moderate
Inferior olives	None	None	None	None
Atrophy of pons greater than cerebellum	Yes	Yes (numeric reduction)	Yes	Yes
Dentate nucleus	Moderate	Severe	Severe	None to mild
Oculomotor nuclei	Unknown	Moderate	Severe	Unknown
Substantia nigra	Mild	Moderate	Moderate	Mild
Pallidum	Unknown	Moderate (internal = external)	Moderate (internal > external)	Mild
Subthalamic nucleus	Unknown	Unknown	Moderate	Mild

*In all cases, brainstem and spinal cord atrophy were greater than cerebellar atrophy and cerebellar atrophy was greater than cerebral atrophy.

same kindred.[44] The SPD phenotype in some families was finally found to be linked to the same genetic abnormality as MJD.[45] It is therefore probable that common clinicopathological features of SPD and HAC, lumped as mossy-fiber type cerebellipetal degeneration,[19] could be applied to MJD, suggesting that these entities are to be grouped under the same diagnostic flag.

In addition to the involvement of the dentate nucleus, further examination of the histological preparations verified that the oculomotor nucleus, pars compacta of substantia nigra, and pallidum were also affected, as observed in MJD[20-24,35] and also in SPD.[38-40,43] No slides were available to examine the subthalamic nucleus. Although unstained sections are not available for immunohistochemical examination, a Nissl-stained section of the internal pallidum contained a neuron harboring a spherical structure distinct from the nucleolus (Figure 3G), which seems identical to the intranuclear inclusion seen in most CAG triplet expansion diseases including MJD.[16-18]

The proposal of Pierre Marie to isolate, from Friedreich ataxia, a group of hereditary ataxias that could be identified on the basis of retained or exaggerated tendon reflexes was really prescient. It proved to be premature, in retrospect, because it was only based on clinical signs that are known today to be present in a variety of entities that genetic tools can now distinguish. Although it is hard to define HAC in the present nosological framework of hereditary ataxias, the clinical and pathological phenotype described in patients from the Haudebourg family is one of the major prototypes of HAC. Clinical and pathological features of this autopsy case are shared with patients from the Haudebourg family, which authorized the diagnosis of HAC, as interpreted in 1943. On the other hand, retrospective review of the clinicopathological features confirmed that the phenotype of this patient is also indistinguishable from that of individuals with MJD. It seems, then, very probable that MJD reported as if it were a new disease entity might have been a description of another clinicopathological aspect of patients from the Haudebourg family with special reference to lesions in the brainstem and basal ganglia. A series of autopsy reports on the patients from the Haudebourg family mainly dealt with spinal cord lesions,[8-11,46] whereas early pathological description of MJD paid more attention to lesions in the basal ganglia and brainstem.[22-24] It is therefore probable that these 2 different aspects were considered to represent different diseases when they were, in reality, 2 different aspects of a single disease.

This autopsy case labeled with the diagnosis of HAC provided us with an opportunity to see how French neurologists and neuropathologists defined HAC in 1943 and to compare the findings with those of MJD. Although it is still debated whether HAC should be limited to a single disease entity, it seems likely that the HAC of Pierre Marie, and more specifically the Haudebourg family, includes clinicopathological characteristics indistinguishable from MJD.

Accepted for publication May 27, 2003.

Corresponding author and reprints: Charles Duyckaerts, MD, PhD, Laboratoire Raymond Escourolle, Service de Neuropathologie, Association Claude Bernard, Groupe Hospitalier, Pitié-Salpêtrière, 47 Bd de l'Hôpital, Cedex 13, Paris 75651, France (e-mail: charles.duyckaerts@psl.ap-hop-paris.fr).

REFERENCES

1. Marie P. Sur l'hérédo-ataxie cérébelleuse. *Sem Med.* 1893;13:444-447.
2. Trouillas P, Robert JM, Aimard G. Le cadre de l'hérédo-ataxie de Pierre Marie doit-il être conservé? *Lyon Med.* 1972;227:1105-1116.
3. Klippel M, Durante G. Contribution à l'étude des affections nerveuses familiales et héréditaires. *Rev Med.* 1892;12:745-786.
4. Brown S. On hereditary ataxy, with a series of twenty-one autopsy cases. *Brain.* 1892;15:250-282.
5. Fraser D. Defect of the cerebellum occurring in a brother and sister. *Glasgow Med J.* 1880;13:199.
6. Nonne M. Über eine eigenthümliche familiäre Erkrankungsform des Centralnervensystems. *Arch Psychiatr Nervenkr.* 1891;22:283-316.
7. Ladame P. Friedreich's disease. *Brain.* 1890;13:467-537.
8. Rydel A. Sur l'anatomie pathologique d'une forme d'hérédo-ataxie cérébelleuse. *Nouv Icon Salpêtrière.* 1904;17:289-303.

9. Switalski. Sur l'anatomie pathologique de l'hérédo-ataxie cérébelleuse. *Nouv Icon Salpêtrière.* 1901; 14:373-387.
10. Thomas A, Roux J-C. Sur une forme d' hérédo-ataxie cérébelleuse: a propos d'une observation suivie d'autopsie. *Rev Med.* 1901;21:762-792.
11. Guillain G, Bertrand I, Godet-Guillain J. Etude anatomique d'un cas d' hérédo-ataxie cérébelleuse. *Rev Neurol.* 1941;73:609-611.
12. Ben-Hamida M, Attira-Romdhane N, Triki CH, Oueslati S, Hentati F. Analyse clinique et génétiquede 188 familles d'hérédo-dégénérescence spino-cérébelleuse: maladies de Friedreich et hérédo-ataxies de P Marie. *Rev Neurol.* 1991;147: 798-808.
13. Ishino H, Sato M, Mii T, et al. An autopsy case of Marie's hereditary ataxia [in Japanese]. *Seishin shinkeigaku zasshi.* 1971;73:747-757.
14. Kurachi M, Shibata T, Koyama Y, Isaki K, Yamaguchi N. Marie's ataxia with nuclear external ophthalmoplegia and muscle atrophy of lower extremities: report of an autopsy case and its family [in Japanese]. *Seishin shinkeigaku zasshi.* 1977; 79:1-25.
15. Matsuyama H, Shimizu K, Katayama T, Fujita R, Goto Y. A case report of the hereditary ataxia [in Japanese]. *Rinsho Shinkeigaku.* 1961;1:146-150.
16. Paulson HL, Perez MK, Trottier Y, et al. Intranuclear inclusions of expanded polyglutamine protein in spinocerebellar ataxia type 3. *Neuron.* 1997; 19:333-344.
17. Fujigasaki H, Uchihara T, Koyano S, et al. Ataxin-3 is translocated into the nucleus for the formation of intranuclear inclusions in normal and Machado-Joseph disease brains. *Exp Neurol.* 2000;165: 248-256.
18. Uchihara T, Fujigasaki H, Koyano S, Nakamura A, Yagishita S, Iwabuchi K. Non-expanded polyglutamine proteins in intranuclear inclusions of hereditary ataxias: triple-labeling immunofluorescence study. *Acta Neuropathol.* 2001;102:149-152.
19. Iwata M. Pierre Marie's hérédo-ataxie cérébelleuse: historical background and current reappraisal [in Japanese]. *Shinkei Naika.* 1980;13:77-84.
20. Iwabuchi K, Tsuchiya K, Uchihara T, Yagishita S. Autosomal dominant spinocerebellar degenerations: clinical, pathological, and genetic correlations. *Rev Neurol.* 1999;155:255-270.
21. Coutinho P, Andrade C. Autosomal dominant system degeneration in Portuguese families of the Azores Islands: a new genetic disorder involving cerebellar, pyramidal, extrapyramidal and spinal cord motor functions. *Neurology.* 1978;28:703-709.
22. Nakano KK, Dawson DM, Spence A. Machado disease: a hereditary ataxia in Portuguese emigrants to Massachusetts. *Neurology.* 1972;22:49-55.
23. Rosenberg RN, Nyhan WL, Bay C, Shore P. Autosomal dominant striatonigral degeneration: a clinical, pathologic, and biochemical study of a new genetic disorder. *Neurology.* 1976;26:703-714.
24. Woods BT, Schaumburg HH. Nigro-spino-dentatal degeneration with nuclear ophthalmoplegia: a unique and partially treatable clinico-pathological entity. *J Neurol Sci.* 1972;17:149-166.
25. Bürk K, Abele M, Fetter M, et al. Autosomal dominant cerebellar ataxia type, I: clinical features and MRI in families with SCA1, SCA2 and SCA3. *Brain.* 1996;119:1497-1505.
26. Dawson DM, Feudo P, Zubick HH, Rosenberg R, Fowler H. Electro-oculographic findings in Machado-Joseph disease. *Neurology.* 1982;32: 1272-1276.
27. Murofushi T, Mizuno M, Hayashida T, et al. Neuro-ototological and neuropathological findings in two cases with Machado-Joseph disease. *Acta Otolaryngol Suppl.* 1995;520(pt 1):136-139.
28. Harding A. The clinical features and classification of the late onset dominant cerebellar ataxias: a study on eleven families including descendants of the "Drew family of Walworth." *Brain.* 1982;105:1-28.
29. Harding A. Classification of the hereditary ataxias and paraplegias. *Lancet.* 1983;1:1151-1155.
30. David G, Abbas N, Stevanin G, et al. Cloning of the SCA7 gene reveals a highly unstable CAG repeat expansion. *Nat Genet.* 1997;17:65-70.
31. Martin J-J, Van Regemorter N, Krols L, et al. On an autosomal dominant form of retinal-cerebellar degeneration: an autopsy study of five patients in one family. *Acta Neuropathol.* 1994;88:277-286.
32. Martin J-J, Van Regemorter N, Del-Favero J, Löfgren A, Van Broeckhoven C. Spinocerebellar ataxia type 7 (SCA7)—correlations between phenotype and genotype in one large Belgian family. *J Neurol Sci.* 1999;168:37-46.
33. Jardim LB, Pereira ML, Siverira I, Ferro A, Sequeiros J, Giugliani R. Neurologic findings in Machado-Joseph disease: relation with disease duration, subtypes and (CAG)n. *Arch Neurol.* 2001; 58:899-904.
34. Miura K. Über "l'hérédo-ataxie cérébelleuse" Marie's: Mitteilungen aus der medicale Fakultät der Kaiserlich-Japanischen Universität zu Tokio. *Mitteil Med Fakult Univ Tokio.* 1898;4:19-47.
35. Tsuchiya K, Wakabayashi M, Oyanagi S, et al. Machado-Joseph disease in Japan: clinicopathological study of 6 autopsy cases with special reference to the clinicopathological correlation to cerebellar ataxia and lower motor neuron signs. *Neuropathology.* 1994;14:13-36.
36. Yuasa T, Ohama E, Harayama H, et al. Joseph's disease: clinical and pathological studies in a Japanese family. *Ann Neurol.* 1986;19:152-157.
37. Meyer A. The morbid anatomy of a case of hereditary ataxia: No. VI of Dr Sanger Brown's series of cases. *Brain.* 1897;20:276-289.
38. Boller F, Seggara JM. Spinopontine degeneration. *Eur Neurol.* 1969;2:356-373.
39. Taniguchi R, Konigsmark BW. Dominant spinopontine atrophy: report of a family through three generations. *Brain.* 1971;94:349-358.
40. Pogacar S, Ambler M, Conklin WJ, O'Neil WA, Lee HY. Dominant spinopontine atrophy. *Arch Neurol.* 1978;35:156-162.
41. Boller F, Seggara JM. Spino-pontine degeneration. In: Vinken PJ, Bruyn GW, eds. *Handbook of Clinical Neurology.* Amsterdam, the Netherlands: North Holland Publishing Co; 1975:389-402.
42. Boller F, Seggara JM. Dominant spinopontine atrophy. *Arch Neurol.* 1979;36:255.
43. Eto K, Sumi SM, Bird TD, McEvoy-Bush T, Boehnke M, Schellenberg G. Family with dominantly inherited ataxia, amyotrophy, and peripheral sensory loss. *Arch Neurol.* 1990;47:968-974.
44. Sequeiros J, Suite NDA. Spinopontine atrophy disputed as a separate entity: the first description of Machado-Joseph disease. *Neurology.* 1986;36: 1408.
45. Higgins JJ, Nee LE, Vasconcelos O, et al. Mutations in American families with spinocerebellar ataxia (SCA) type 3: SCA3 is allelec to Machado-Joseph disease. *Neurology.* 1996;46:208-213.
46. Marie P, Foix C. Lésion médullaires dans quatre cas d'hérédoataxie cérébelleuse. *Rev Neurol.* 1914; 30:797-798.

ELSEVIER

Journal of Neuroscience Methods 135 (2004) 67–70

JOURNAL OF NEUROSCIENCE METHODS

www.elsevier.com/locate/jneumeth

Dual enhancement of triple immunofluorescence using two antibodies from the same species

Ayako Nakamura, Toshiki Uchihara*

Department of Neuropathology, Tokyo Metropolitan Institute for Neuroscience, 2-6 Musashi-dai, Fuchu, Tokyo 183-8526, Japan

Received 15 November 2003; received in revised form 9 December 2003; accepted 11 December 2003

Abstract

Triple immunofluorescence method with two mouse monoclonal antibodies and another rabbit polyclonal antibody was established with catalyzed reporter deposition (CARD) amplification on thick floating sections from the rat cerebellum. One of the monoclonal antibodies (anti-calbindin), diluted maximally, probed with anti-mouse IgG–horseradish peroxidase (HRP) and amplified with Cy5-conjugated tyramide, immunolabeled cerebellar Purkinje cells and their arborization. Subsequently, a rabbit polyclonal IgG (anti-glial fibrillary acidic protein (anti-GFAP)), probed with anti-rabbit IgG–HRP, amplified with biotin–tyramide and visualized with fluorescein-isothiocyanate (FITC)–streptavidin, immunolabeled Bergmann's glia. Another mouse monoclonal IgG (anti-SNAP25), probed with anti-mouse IgG–rhodamine without CARD amplification, selectively visualized synaptic sites, because the maximal dilution of the other monoclonal antibody (anti-calbindin) was below the detection threshold of this anti-mouse IgG–rhodamine. Separation of the two signals (calbindin and SNAP25), each detected through mouse monoclonal antibody, was then based on the difference of sensitivity either with or without CARD amplification. Triple immunofluorescence is possible when just one of the three primary antibodies is from different species. Intensification of two of the three signals provides further advantages to examine immunolocalization of multiple epitopes on histological sections.

Keywords: Catalyzed reported deposition; Multilabeling; Tyramide; Cerebellum; Development

1. Introduction

Multifluorolabeling immunohistochemistry is an indispensable tool to examine spatial relationship between epitopes on histological sections. It requires a clear separation of signals and sufficient intensity of each signal. Because the signals obtained with conventional fluorochromes conjugated with secondary antibodies are not always intense enough, several signal amplification methods have been developed. Among them, catalyzed reporter deposition (CARD) method is now frequently used as one of the methods of choice (Adams, 1992; Bobrow et al., 1989). Amplification with CARD method is mediated by horseradish peroxidase (HRP), usually conjugated with secondary antibodies and reacted with tyramide in the presence of hydrogen peroxide. This yields amplified signal represented by a reporter molecule, such as biotin or fluorochrome, conjugated in advance with tyramide, that accumulates around HRP (Adams, 1992; Bobrow et al., 1989). Signal amplification with CARD method allows further dilution of the primary antibody below the threshold detectable with non-amplified conventional method using fluorochrome-labeled secondary antibodies (Kumar et al., 1999; Speel et al., 1997; van Gijlswijk et al., 1997). Hunyaday et al. (1996) first reported that a combination of this highly sensitive method with conventional fluorolabeling enabled double immunolabeling based on this difference in the detection threshold even when the two epitopes were probed with primary antibodies of the same class from the same species. This double labeling with antibodies from the same species can be combined with an additional antibody from another species without danger of cross-reaction, as we demonstrated recently (Uchihara et al., 2003). Moreover, by using tyramide-conjugated fluorochromes, it is possible to amplify two immunofluorescent signals from two antibodies from different species (Uchihara et al., 2000). Because this dual amplification allows further dilution of these two primary antibodies, it can be theoretically combined with

* Corresponding author. Tel.: +81-42-325-3881/4712; fax: +81-42-321-8678.
E-mail address: uchihara@tmin.ac.jp (T. Uchihara).

0165-0270/$ – see front matter © 2004 Elsevier B.V. All rights reserved.
doi:10.1016/j.jneumeth.2003.12.003

an additional primary antibody (the third antibody) from either species. A fluorochorome-labeled secondary antibody that visualizes the third antibody is not sensitive enough to immunolabel the diluted primary antibodies that have been already visualized. Triple labeling achieved in this way, therefore, involves two antibodies from the same species, one of which should be amplified, and another antibody from different species, that can also be amplified. In this study, we used, as primary antibodies, two mouse monoclonal IgGs and a rabbit polyclonal IgG to perform triple labeling. Amplification of the signal from the rabbit polyclonal IgG and another from one of the two mouse monoclonal IgGs yielded signals intense enough to be detected in the thick sections.

2. Materials and methods

Wistar rats at postnatal day 14 (P14) were perfused transcardially with Zamboni fixative under anesthesia with inhaled diethyl ether followed by intraperitoneal administration of pentobarbital (60 mg/kg). The cerebella were taken immediately and further immersed in the same fixative overnight. After being rinsed in phosphate-buffered saline (PBS), the fixed tissues were cryoprotected by immersion in 20% sucrose in 0.1 M phosphate buffer. Floating sections with a thickness of 30 μm were obtained on a freezing microtome. Endogenous peroxidases were thoroughly inactivated by treating the sections with 2% hydrogen peroxide in PBS for 30 min. Then the sections were incubated with 5% bovine serum albumin diluted in PBS for 30 min. They were then incubated with anti-calbindin mouse monoclonal antibody of IgG class (1:2000, Swant, Bellinzona, Switzerland) at 4 °C for 3 days. In order to determine this concentration of the anti-calbindin antibody, serially diluted antibody was tested (data not shown) either with or without CARD amplification (Uchihara et al., 2003). This concentration was chosen so that the corresponding immunofluorescent signal was detectable only after CARD amplification but not without this amplification. Sections were then incubated with anti-mouse IgG made in goat conjugated with HRP (1:1000, Kirkegaard and Perry, Gaithersburg, MD). The HRP signal was intensified and visualized with tyramide conjugated with Cy5 (1:200, Perkin-Elmer, Boston, MA). Subsequent procedures were undertaken in the dark. Residual HRP was inactivated by incubating the sections in 1% hydrogen peroxide for 20 min. They were then incubated with the mixture of anti-glial fibrillary acidic protein (anti-GFAP) rabbit polyclonal antibody of IgG class (1:5000, DAKO, Glostrup, Denmark) and anti-SNAP25 mouse monoclonal antibody of IgG class (a marker for synaptic protein, SMI 81, 1:3000, Sternberger Monoclonal, Lutherville, MD) at 4 °C for another 2 days. This concentration of the anti-SNAP25 antibody was sufficient to be visualized without CARD amplification (Uchihara et al., 2003). Sections were then incubated with anti-rabbit IgG made in goat conjugated with HRP (1:500, Pierce, Rockford, IL). They were then incubated with biotinylated tyramide (1:1000, Perkin-Elmer; Adams, 1992) and the amplified signal was visualized with fluorescein-isothiocyanate (FITC) conjugated with streptavidin (1:200, Vector, Burlingame, CA). The SNAP25 epitope was visualized conventionally in parallel with an anti-mouse IgG made in sheep conjugated with rhodamine red (1:200, Jackson ImmunoRes, West Grove, PA). This anti-mouse IgG conjugated with rhodamine red visualized the anti-SNAP25 antibody at this concentration (1:3000) as determined as earlier but was not sensitive enough to visualize the anti-calbindin antibody diluted to 1:2000 (data not shown). Sections were mounted with 90% glycerol in 0.1 M phosphate buffer containing 0.1% of *p*-phenylenediamine and were observed under a confocal laser scanning microscope (Leica TCS/SP, Heidelberg, Germany). For excitation of fluorochromes, an argon–krypton laser is combined with an acoustico-optical tunable filter system, which can adjust the individual intensity of each of the three laser beams (488, 568 and 647 nm) independently. Relationship between these epitopes, probing antibodies, the corresponding fluorochromes and their excitation and emission wavelengths are shown in Table 1.

3. Results

Fig. 1 shows the triple-fluorolabeled images of the rat cerebellum at P14. Although two (calbindin: C, blue; SNAP25: B, red) of the three epitopes were probed with anti-mouse IgG of the same class, there was practically no overlap between the fluorescent signals. Each signal was captured independently and emission peak of each, measured with spectrophotometer (Leica TCS/SP), was not different from that expected from each fluorochrome used, as shown in Table 1. This confirmed that the detection

Table 1
Fluorescent dyes and their link to epitopes

Dye	Excitation wavelength (nm)	Detection range (nm)	Secondary antibody–reporter molecule	Target epitope	Color displayed
FITC–str	488	500–530	Anti-rabbit IgG–HRP[a]	GFAP	Green
Rd	568	590–630	Anti-mouse IgG–Rd	SNAP25	Red
Cy5–tyr	647	700–750	Anti-mouse IgG–HRP[a]	Calbindin	Blue

FITC: fluorescein-isothiocyanate; str: streptavidin; HRP: horseradish peroxidase; Rd: rhodamine red; tyr: tyramide.
[a] Amplified.

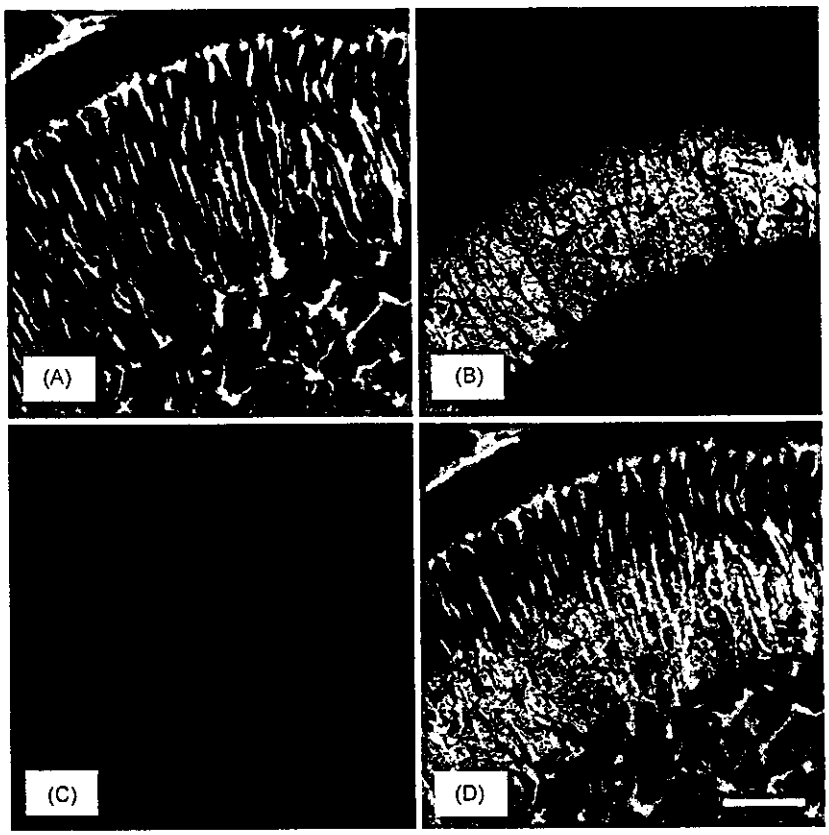

Fig. 1. Floating section (30 μm thick) from a rat cerebellum at postnatal day 14. (A) Glial fibrillary acidic protein epitope enhanced with biotinylated tyramide and visualized with streptavidin–FITC. Bergmann's glia and their processes are labeled. (B) SNAP25, a synaptic protein, probed with a mouse monoclonal antibody of IgG class without amplification through rhodamine red. (C) Calbindin probed with the other mouse monoclonal antibody of IgG class amplified and detected with tyramide–Cy5. Note the absence of cross-talk between the three immunofluorescent signals. (D) Merged image of (A)–(C) (bar = 50 μm).

system clearly distinguished each fluorochrome without cross-talk. Indeed, three different signals represented expected structures, that did not overlap with one another. Calbindin localized to Purkinje cell cytoplasm and its arborization was visualized through Cy5 (C, blue), anti-GFAP localized to Bergmann's glia and their processes was visualized through FITC (A, green) and SNAP25 in synapses accumulated in the molecular layer was visualized through rhodamine red (B, red). The merged image (D) also confirmed the absence of overlap between these signals. Omission of any of the primary antibodies was associated with disappearance of the corresponding signal (data not shown). Reversed assignment of FITC and Cy5 gave essentially the same results (data not shown). Similar triple-labeled images can be obtained at any depth of the 30 μm thick sections.

4. Discussion

We successfully performed triple immunofluorescence with two antibodies of mouse monoclonal IgG and another antibody of rabbit polyclonal IgG. Amplifying one (calbindin) of the two signals with the CARD method enabled to dilute this antibody (anti-calbindin, usually more than another 10-fold) below the threshold (Uchihara et al., 2000, 2003) that is detectable directly with the conventional secondary anti-mouse IgG conjugated with rhodamine red. This enabled to distinguish two mouse monoclonal IgGs, even though these two were probed with anti-mouse IgG. Sharp separation of signals in multiple immunolabeling is usually achieved by using primary antibodies from different species. Appropriate combination, however, is not always available, and one may be confronted with further difficulty especially when dealing with triple immunolabeling. Therefore, double labeling with two primary antibodies from the same species and class, for example, two mouse monoclonal IgGs as we demonstrated in this study, may be of great help. Direct conjugation of biotin to one of the primary antibodies may be one of the methods of choice for this purpose, but the procedure is cumbersome and requires a relatively large amount of the primary antibody (Uchihara et al., 1995). Hunyaday et al. (1996) was the first who utilized CARD amplification in this way for double fluorolabeling to obtain a good separation from non-amplified signal. Our previous study expanded this procedure by combining the third primary antibody from another species; double labeling with two rabbit polyclonal IgGs using

CARD amplification and another mouse monoclonal IgG was visualized without amplification (Uchihara et al., 2003).

Another difficulty in immunolabeling using fluorochrome-conjugated secondary antibodies is that fluorescent signals are not always sufficiently intense. CARD amplification is now often used to amplify the signal mediated by HRP targeted to the epitope. Usually, the HRP is reacted with tyramide conjugated to a reporter molecule such as biotin. Final visualization is mediated through this biotin to be linked with streptavidin-conjugated fluorochrome or HRP. In a previous study, we demonstrated that dual enhancement of double immunofluorescent signals was possible by using CARD amplification (Uchihara et al., 2000). Possible cross-reaction at the common reporter, HRP, was avoided by inactivating residual HRP with hydrogen peroxide after one of the epitopes was fluorolabeled. Subsequent cross-reaction at another common reporter, biotin, was circumvented by using fluorochromes, that are directly conjugated with tyramide. This eliminated the necessity of streptavidin for coupling between accumulated reporter (for example, biotin) and fluorochrome. Colocalization of two epitopes, ubiquitin and tau, was shown in that study (Uchihara et al., 2000), which confirmed that CARD amplification was suitable also to demonstrate colocalization of epitopes.

In the present study, employment of CARD amplification for triple immunofluorescence brought about at least two advantages; distinction between the two signals from the two mouse monoclonal IgGs and dual amplification of two fluorescent signals, one from mouse monoclonal IgG and the other from rabbit polyclonal IgG. Intensified signals enabled them to be observed throughout the entire thickness (30 μm) of the floating sections. Intensified triple immunofluorescence is now possible when just one of the three primary antibodies is from different species. This method will expand the applicability of triple immunofluorescence for research and diagnosis.

Acknowledgements

Supported in part by the grants (TU) from the Ministry of Health, Labor and Welfare (Longevity Science H-14-005) and from the Ministry of Education, Culture, Sports, Science and Technology (grant-in-aid for Scientific Research B15300118).

References

Adams JC. Biotin amplification of biotin and horseradish peroxidase signals in histochemical stains. J Histochem Cytochem 1992;40:1457–63.

Bobrow MN, Harris TD, Shaughnessy KJ, Litt GJ. Catalyzed reporter deposition, a novel method of signal amplification. Application to immunoassays. J Immunol Methods 1989;125:279–85.

Hunyaday B, Krempels K, Harta G, Mezey É. Immunohistochemical signal amplification by catalyzed reporter deposition and its amplification in double immunostaining. J Histochem Cytochem 1996;44:1353–62.

Kumar RK, Chapple CC, Hunter N. Improved double immunofluorescence for confocal laser scanning microscopy. J Histochem Cytochem 1999;47:1213–7.

Speel EJM, Ramaekers FCS, Hopman AHN. Sensitive multicolor fluorescence in situ hybridization using catalyzed reporter deposition (CARD) amplification. J Histochem Cytochem 1997;45:1439–46.

Uchihara T, Kondo H, Akiyama H, Ikeda K. Single-laser three-color immunolabeling of a histological section by laser scanning microscopy: application to senile plaque-related structures in post-mortem human brain tissue. J Histochem Cytochem 1995;43:103–6.

Uchihara T, Nakamura A, Nagaoka U, Yamazaki M, Mori O. Dual enhancement of double immunofluorescent signals by CARD: participation of ubiquitin during formation of neurofibrillary tangles. Histochem Cell Biol 2000;114:447–51.

Uchihara T, Nakamura A, Nakayama H, Arima K, Ishizuka N, Mori H, et al. Triple immunofluorolabeling with two rabbit polyclonal antibodies and a mouse monoclonal antibody allowing three-dimensional analysis of cotton wool plaques in Alzheimer disease. J Histochem Cytochem 2003;51:1201–6.

van Gijlswijk RPM, Zijlmans HJM, Wiegeant J, Bobrow MN, Erickson TJ, Adler KE, et al. Fluorochrome-labelled tyramides: use in immunocytochemistry and fluorescence in situ hybridization. J Histochem Cytochem 1997;45:375–82.

Acta Neuropathol (2004) 108 : 279–286
DOI 10.1007/s00401-004-0885-4

REGULAR PAPER

Takahiko Umahara · Toshiki Uchihara · Kuniaki Tsuchiya
Ayako Nakamura · Toshihiko Iwamoto · Kenji Ikeda
Masaru Takasaki

14-3-3 proteins and zeta isoform containing neurofibrillary tangles in patients with Alzheimer's disease

Received: 25 November 2003 / Revised: 20 April 2004 / Accepted: 28 April 2004 / Published online: 2 July 2004

Abstract Immunolocalization of 14-3-3 proteins in Alzheimer's disease (AD) brains was investigated using isoform-specific antibodies. Weak granular immunoreactivity of 14-3-3 proteins was found in neuronal cytoplasm in control subjects and AD brains. Both intracellular and extracellular neurofibrillary tangles (NFTs), as well as neuropil thread-like structures, were immunopositive for 14-3-3 proteins. This was corroborated by triple-fluorolabeling method visualizing paired helical filament (PHF) tau and 14-3-3 epitopes in relation to fibrillary state detected by thiazin red. Pretangle neurons (positive for PHF-tau without fibrillary structure detected by thiazin red) only contained fine granular immunoreactivity (IR) of 14-3-3, which was similarly found in unaffected neurons. Granular cytoplasmic IR of 14-3-3 proteins in pretangle neurons was not colocalized to granular tau-like IR, which suggests that participation of 14-3-3 proteins in NFT formation was restricted to its later stages. Its zeta isoform was most prominent in these NFTs, suggesting that this isoform is a major component involved in the formation of NFTs. In contrast, IR of epsilon isoform was found in the neuropil of the hippocampus and that of sigma isoform was localized to granule cells of the dentate gyrus in AD brains, as seen in the age-matched controls. Expression of 14-3-3 proteins were found to be highly variable and dependent on their isoforms, regions and cell types. Molecular, as well as topographical, dissection of 14-3-3 proteins will provide us with an improved understanding of this molecule in normal and pathological conditions.

Keywords 14-3-3 proteins · Zeta isoform · Alzheimer's disease · Neurofibrillary tangles · Tau protein

T. Umahara (✉) · T. Iwamoto · M. Takasaki
Department of Geriatrics, Tokyo Medical University,
6-7-1 Nishi-Shinjyuku, Shinjyuku-ku, 160-0023 Tokyo, Japan
Tel.: +81-3-33426111, Fax: +81-3-33422305,
e-mail: takahiko@tokyo-med.ac.jp

T. Umahara · T. Uchihara · A. Nakamura
Department of Neuropathology,
Tokyo Metropolitan Institute for Neuroscience,
2-6 Musashi-dai, Fuchu, 183-8526 Tokyo, Japan

K. Tsuchiya
Department of Laboratory Medicine and Pathology,
Tokyo Metropolitan Matsuzawa Hospital,
2-1-1 Kamikitazawa, Setagaya-ku, 156-0057 Tokyo, Japan

K. Ikeda
Department of Psychogeriatrics, Tokyo Institute of Psychiatry,
2-1-8 Kamikitazawa, Setagaya-ku, 156-0057 Tokyo, Japan

Introduction

14-3-3 proteins are a family of highly conserved molecule of 30 kDa [6, 9]. The proteins, first detected by Moore and Peres [23] as specific acidic proteins, are mainly localized to the synapses and neuronal cytoplasm. Although they are known as adaptor proteins, which bind to the phosphoserine-containing motifs of the target protein, they are now endowed with a growing series of potential functions and pathological relevance [5, 6, 9, 28, 30].

First, elevated 14-3-3 proteins in the cerebrospinal fluid are one of the potential indicators of transmissible spongiform encephalopathy [11], although that finding was also seen in other diseases [29]. Second, the proteins regulate intercellular signal transduction by modulating phosphorylation of the target proteins [5, 9, 12, 14, 15, 25, 31]. Third, they potentially control apoptosis induced by BAD [28, 37]. Fourth, they are colocalized to deposits, such as Lewy bodies (LBs) [17] or glial cytoplasmic inclusions (GCIs) [18, 19]: both consist of α-synuclein that shares structural homology with 14-3-3 proteins. Finally, their association to tau protein, which is the main component of neurofibrillary tangles (NFTs), first reported by Layfield et al [20] on NFTs of AD brains, was reinforced after Hashiguchi et al. [10] reported that its zeta isoform was an effector of tau phosphorylation. Recently, Agarwal-Mawal and colleagues [1] reported that the 14-3-3 zeta isoform connects glycogen synthase kinase(GSK)-3β to tau within a brain microtubule-associated tau phosphorylation complex.

Although the body of biochemical knowledge on 14-3-3 proteins is still growing and attracting increasing atten-

tion, detailed immunohistochemical studies on diseased human brains are still limited. Moreover, seven isoforms (β, γ, ε, ζ, η τ, and σ) of the protein have been so far identified in mammals [9, 21]. There were several reports concerning possible relevance of isoform specificity for disease [4, 8, 10, 21, 27, 36]. However, the physiological functions or pathological relevance of each isoform have yet to be clarified. This prompted us to investigate immunolocalization of each isoform of the 14-3-3 proteins in relation to NFTs in AD brains.

Multi-fluorolabeling with a fluorochrome, thiazin red (TR), that has an affinity to fibrillary structures such as NFTs [26, 32, 33, 34], clarified stage- and isoform-specific involvement of 14-3-3 proteins in the development of NFTs in AD brains.

Materials and methods

Hippocampal specimens were obtained from four elderly control subjects (67–85 years old) and from six patients with AD (64–83 years old, Braak's stage IV–V [7]). Five-micrometer-thick sections were obtained from formalin-fixed, paraffin-embedded blocks. After being autoclaved in a citrate buffer at 120°C for 20 min, they were treated with 1% hydrogen peroxide for 30 min. Sections were incubated with one of the primary antibodies made in rabbit (Immuno-Biological Laboratories, Gunma, Japan) against human 14-3-3 protein (1:2,000, anti-14-3-3 COM, amino acid sequence used for the epitope: KDSTLIMQLLRDNLT, without distinguishing each isoform) or its each isoform (anti-beta: MTMDKSELVQ, 1:500, anti-gamma: QQDDDGGEGNN, 1:200, anti-epsilon: EQNKEALQDVEDENQ 1:500, anti-zeta: MDKNELVQK 1:200, and anti-sigma: EEGGEAPQEPQS 1:300 isoforms) [36] at 4°C for 2 days. They were then incubated with the appropriate biotinylated secondary antibody for 2 h. After incubation with the avidin-biotin-peroxidase complex (1:1,000, ABC Elite, Vector, Burlingame, CA) for 1 h, peroxidase labeling was visualized with 0.03% 3,3-diaminobenzidine, 0.6% nickel ammonium sulfate, 0.05 M imidazole and 0.00015% hydrogen peroxide. A deep purple immunoreaction product appeared after 15–20 min.

Immunolocalization of 14-3-3 epitopes and their relation to NFTs were investigated with multi-fluorolabeling with one of the anti-14-3-3 antibodies (1:1,600 for 14-4-3 protein COM or 1:200 for anti-zeta isoform) and anti-PHF tau monoclonal antibody (1:1,000, AT8, Innogenetics, Zwijndrecht, Belgium) that recognizes phosphatase-sensitive serine199 and 202 epitopes of tau protein, but does not cross-react with normal tau proteins [22]. 14-3-3 epitopes were probed with an anti-rabbit IgG conjugated with horseradish peroxidase (1:500, Pierce, Rockford, IL) followed by amplification with biotinylated tyramide (1:1,000), and was finally visualized with streptavidin-coupled FTIC (1:200, Kirkegaard and Perry, Gaithersburg, MD). The PHF-tau epitope was simultaneously visualized with Cy5-conjugated anti-mouse IgG (1:200, Chemicon, Temecula, CA). The double-labeled sections were then immersed in 0.01 M phosphate-buffered saline containing a fluorochrome, thiazin red (TR, 1:30,000, Wako, Tokyo, Japan) that binds to fibrillary structures like NFTs [26, 32].

Sections were observed under a epifluorescence microscope combined with laser confocal system (TCS-SP, Leica, Heidelberg, Germany). FITC (emission peak: 518 nm) was detected through a 500- to 540-nm light path. TR (emission peak: 620 nm) was excited by a laser beam of 568 nm from an Ar-Kr laser and its emission was detected through 600- to 640-nm light path. Emission from Cy-5 (emission peak: 667 nm) was detected through a 660- to 730-nm light path. Each of the fluorescence signals was considered positive when it was more intense than the autofluorescence of lipofuscin granules.

After triple-stained images had been recorded, the same section was subjected to the Gallyas staining. Comparing the same field enabled the relationship between four different staining features [32, 33, 34].

Protein extraction and Western blot analyses

Extraction and Western blotting were performed as described previously [3]. Briefly, AD and control brains were homogenized and then fixed by 10% trichloroacetic acid. Each pellet was resuspended by sonication in a sample buffer containing 9 mol/l urea, 2% Triton X, and 5% 2-mercaptoethanol. Then, one fifth volume of 10% lithium dodecyl sulfate solution and approximately 2 µl of 1 mol/l TRIS solution were added to sample buffer, and the samples were sonicated again.

Lysates containing equal amounts of protein (10 µg) were subjected to 10% sodium dodecyl sulfate-polyacrylamide gel electrophoresis. Proteins were then transferred to a polyvinylidene difluoride membrane. The blots were blocked with 10%(wt/vol) skim milk and 0.1% Tween 20 in TRIS-buffered saline (TBS) at room temperature for 1 h and washed. The blots were then probed with anti-14-3-3 COM (1:2,000) or anti-14-3-3 zeta isoform (1:1,000) antibody in 1% bovine serum albumin/TBS solution at 4°C for 3 days. After three washes with 1% (wt/vol) skim milk and 0.1% Tween 20 in TBS at room temperature for 30 min, the blots were incubated with horseradish peroxidase-coupled goat anti-rabbit IgG secondary antibody (Pierce) diluted 1:4,000 with 1% (wt/vol) skim milk/TBS at room temperature for 2 h. The blots were washed three times with 0.1% Tween 20 in TBS, and visualized with the use of an enhanced chemiluminescence system (Amersham, Arlington Heights, IL).

Results

Western blot analyses

Probing human brain extracts with the anti-14-3-3 COM and zeta isoform on Western blot (Fig. 1) demonstrated a

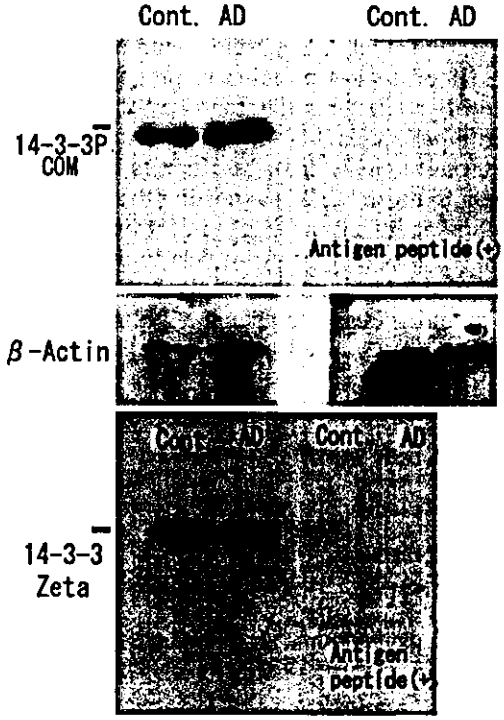

Fig. 1 Western blot of extracts from human control subject (*Cont*) and Alzheimer's disease (*AD*) brains probed with anti-14-3-3 protein (COM) and anti-zeta isoform. 14-3-3 proteins-immunoreactive bands of approximately 30 kDa are observed. *Right lanes*: spceificity control, with antibody incubated with the antigen peptide. β-Actin-immunoreactive bands are shown as control (molecular weight marker 42 kDa)

Fig. 2 14-3-3 COM IR in hippocampal sections from elderly control subjects, weak granular 14-3-3-like IR is observed in neuronal somata (*arrows*) and processes (*arrowheads*) of some hippocampal pyramidal neurons in all cases (*IR* immunoreactivity). *Bar* 100 μm

major band at approximately 30 kDa in control and AD brain. These immunopositive bands were abolished when each antigenic peptide was added to the solution containing the primary antibodies.

Fig. 3 NFTs and neuropil thread-like structures probed with anti-14-3-3 COM antibody in hippocampal sections from AD brains. **A** Many 14-3-3-immunoreactive NFTs. **B** Weak granular IR observed in neuronal somata. **C** Intracellular NFT, harboring a neuronal nucleus. **D** Extracellular NFT. **E** Neuropil threads-like structures intensely stained with the anti-14-3-3 COM (*NFT* neurofibrillary tangle). *Bars* **A** 100 μm; **B–E** 10 μm

Immunohistochemistry

In hippocampal sections from elderly control subjects, weak granular 14-3-3-like immunoreactivity (IR) (anti-14-3-3 COM) was observed in neuronal somata and processes of some hippocampal pyramidal neurons in all cases (Fig. 2).

In the hippocampus of AD brains, the anti-14-3-3 COM antibody immunolabeled some neurons and many NFTs (Fig. 3A). Weak granular IR was observed in some neurons (Fig. 3B). Although its intensity varied greatly, some intracellular (I-) NFTs (Fig. 3C), with tight fibrillary structure with apparently remaining nucleus [6], were strongly immunopositive for 14-3-3 proteins. IR of neuronal somata in cells that had NFTs was similar to IR of neurons that did not have NFTs. A lot of extracellular (E-) NFTs (Fig. 3D), presumably represented by thick, widely separated parallel bundles not accompanied by nucleus, were immunolabeled with this antibody, although its intensity were less intense than that of I-NFTs. In both I- and E-NFTs, this 14-3-3-like IR was not restricted to perinuclear region and extended to entire structure of NFTs. Although neuronal processes were weakly immunolabeled with the anti-14-3-3 COM antibody, strongly immunoreactive thread-like structures were observed in AD brains (Fig. 3E).

Immunohistochemical labeling was abolished when the primary antibody 14-3-3 COM and zeta isoform was coincubated with the corresponding antigen peptide (Fig. 4). We failed to demonstrate 14-3-3-like IR in senile plaques.

When probed with either anti-beta, anti-gamma or anti-zeta isoform-specific antibody against 14-3-3, NFTs in AD brains, as well as neurons in controls, exhibited immunostaining pattern similar to that observed with the anti-14-3-3 COM. Among them, labeling with anti-zeta isoform was most intense (Fig. 5A), while NFTs immunolabeled with antibodies specific for other isoforms were limited in number (data not shown).

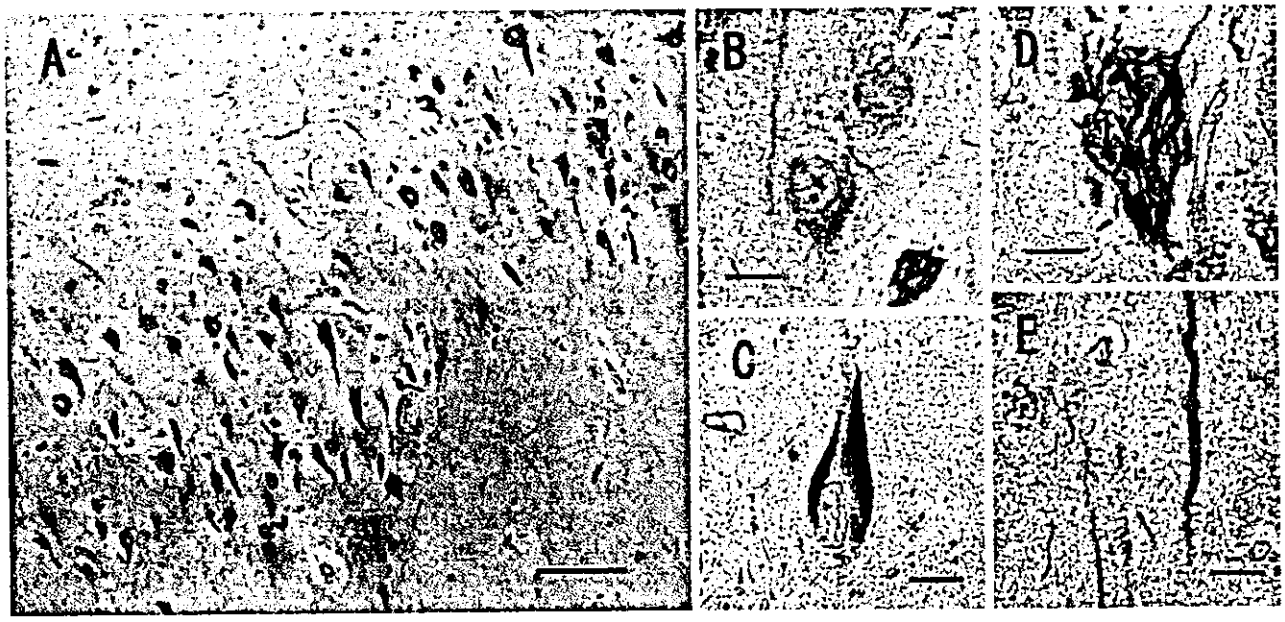

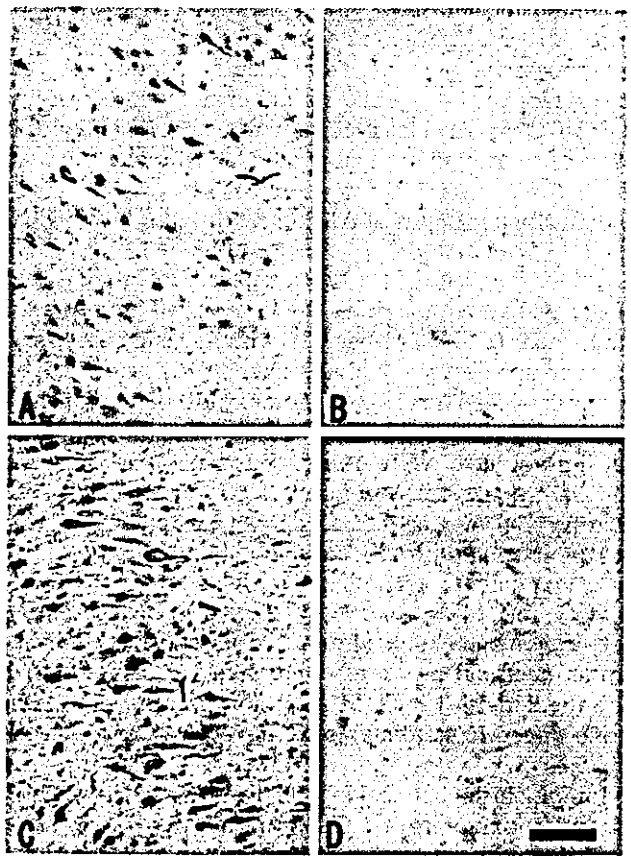

Fig. 4 **A** 14-3-3 COM-immunoreactive NFTs. **B** Immunohistochemical labeling is abolished when the primary antibody (14-3-3 COM) is coincubated with the corresponding antigen peptide. **C** Zeta isoform-immunoreactive NFTs. **D** Immunohistochemical labeling is abolished when the primary antibody (zeta isoform) is coincubated with the corresponding antigen peptide. *Bar* 100 μm

Granule cells in the dentate gyrus were intensely stained with the anti-sigma antibody both in control and AD brains (Fig. 5B). NFTs (Fig. 5B, arrow) in these granule cells were also immunostained with this antibody. Neuropil of the cerebral cortex was homogeneously stained with the anti-epsilon antibody, while neuronal soma was relatively spared (Fig. 5C). The number of NFTs labeled by this anti-epsilon antibody was limited. Some glial cells in the white matter of AD brains were also stained with this anti-epsilon antibody (Fig. 5D).

Multi-fluorolabeling study

Figure 6 shows immunolocalization of 14-3-3 COM (FITC: green) PHF-tau (AT8-Cy5: blue) and of their relation to NFTs (TR: red) in hippocampal pyramidal neurons. 14-3-3 proteins was colocalized to PHF tau and fibrillary structures of NFT (detected by thiazin red and Gallyas staining).

However, some pretangle neurons (positive for AT8 without fibrillary structure detected by thiazin red) were not immunostained with anti-14-3-3 COM antibodies (Fig. 7A). Fig. 7D shows a difference in the staining profile between a pretangle neuron, an unaffected neuron, and an NFT. This pretangle neuron only has fine granules immunolabeled with the anti-14-3-3 COM antibody, which is similarly found in unaffected neurons. Pretangle neurons have no more than few fine granules immunolabeled with this antibody.

Discussion

The present study demonstrated immunolocalization of different isoforms of 14-3-3 protein in relation to NFTs. A previous report by Layfield et al. [20] demonstrated that 14-3-3-like IR was more intense in perinuclear portion of NFTs. The present study demonstrated, in contrast, that 14-3-3-like IR was not restricted to the perinuclear portion of NFT, but was extended to the entire NFT and to neuropil threads. The antibodies used in the present study probed a single band of 30 kDa that corresponds to an expected molecular mass of 14-3-3 protein on Western blot. Immunohistochemical labeling, as well as the immunoreactive bands on Western blot, was abolished when the primary antibody was coincubated with the corresponding antigen peptide. This confirmed the specificity of the antibodies on both Western blot and immunohistochemistry. Our findings based on the antibody with documented specificity provides firm evidence that some epitopes on 14-3-3 protein are not restricted to perinuclear portion. This was further corroborated by immunolocalization of the zeta-isoform of 14-3-3 protein, again not restricted to perinuclear portion, but extended to the entire portion of NFT. Colocalization of 14-3-3 to the entire portion of NFTs was further confirmed by multi-labeling method with PHF-tau.

It has been reported that 14-3-3 protein, especially its zeta isoform, potentially binds to the microtubule-binding region of tau, regardless of phosphorylation state of tau [10]. In addition to binding of zeta isoform to tau, it potentially stimulates phosphorylation of recombinant tau by activating protein kinase A and neuronal cdc2-like kinase. Another report [1] suggests that zeta isoform dimer simultaneously binds and bridges tau and GSK3βand stimulates GSK3β-catalyzed tau phosphorylation.

One of the possibilities may be that binding of 14-3-3 protein to tau may facilitate tau phosphorylation probably at early stage of tau accumulation, that probably occurs after phosphorylation in AD brain. Our multi-labeling immunohistochemistry, however, demonstrated that it was fibrillary NFTs that were associated with 14-3-3-like IR. It failed to demonstrate 14-3-3-like IR in tau deposition not associated with fibrillary structure (so-called pretangles, as demonstrated by tau-like IR without TR staining) [32, 33, 34]. If these non-fibrillar tau-deposits represent early stage of NFT formation, the immunohistochemical findings in the present study is not compatible with possible participation of 14-3-3 in tau phosphorylation at least in the early stage of NFT formation. Association of 14-3-3 proteins to fibrillar tau deposits as NFT may suggest potential roles of this protein either in later stage of NFT for-

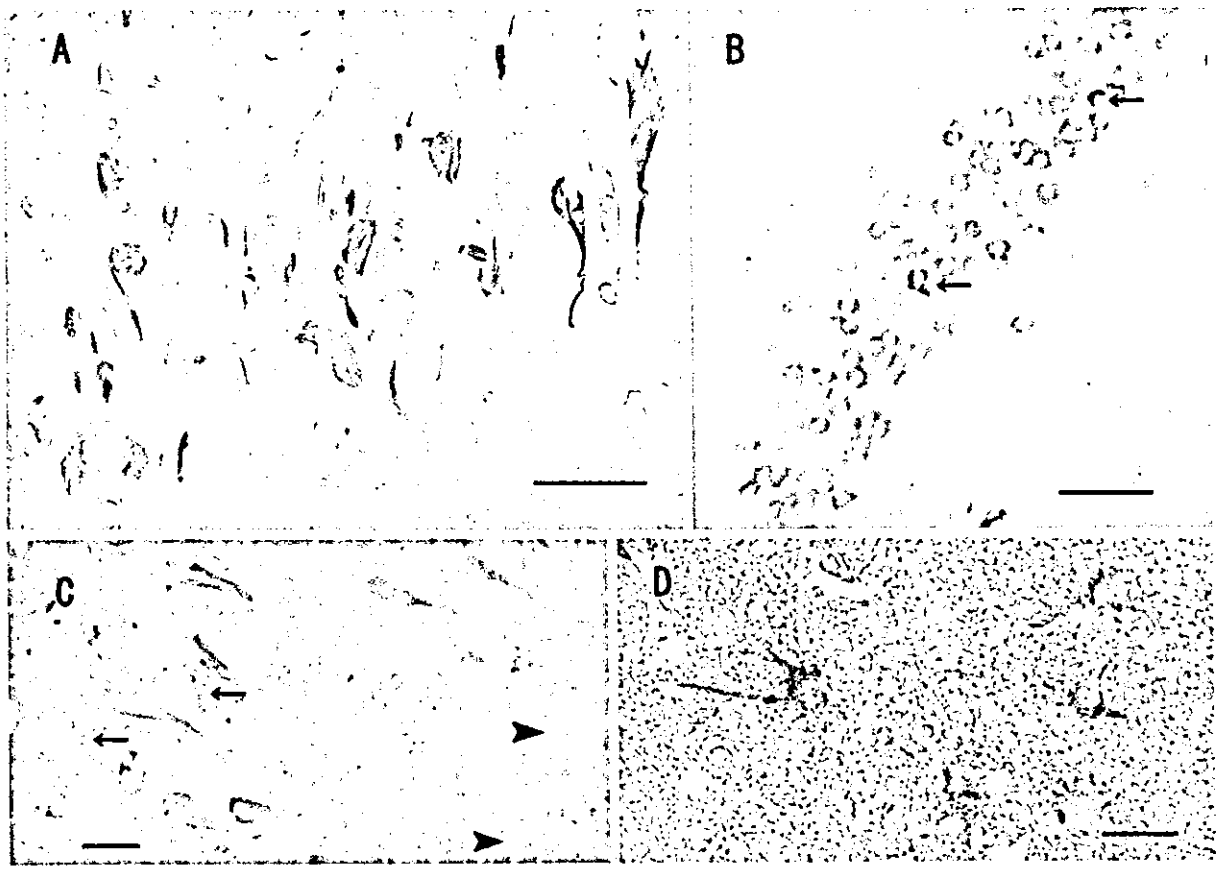

Fig. 5 Immunolocalization of zeta, sigma and epsilon isoforms of 14-3-3 proteins. **A** Zeta isoform-containing NFTs in hippocampal sections from AD brains. **B** Granule cells in the dentate gyrus are stained with the anti-sigma isoform antibody in AD brain. NFTs in granular cells in the dentate gyrus are strongly stained (*arrows*). **C** Neuropil of the hippocampus are homogeneously stained with the anti-epsilon isoform antibody, while neurons (*arrows*) and process (*arrowheads*) are relatively spared. **D** Some glial cells in the white matter of AD brains are also positive for the epsilon isoform. **A**, **B**, **D** 50 μm; **C** 20 μm

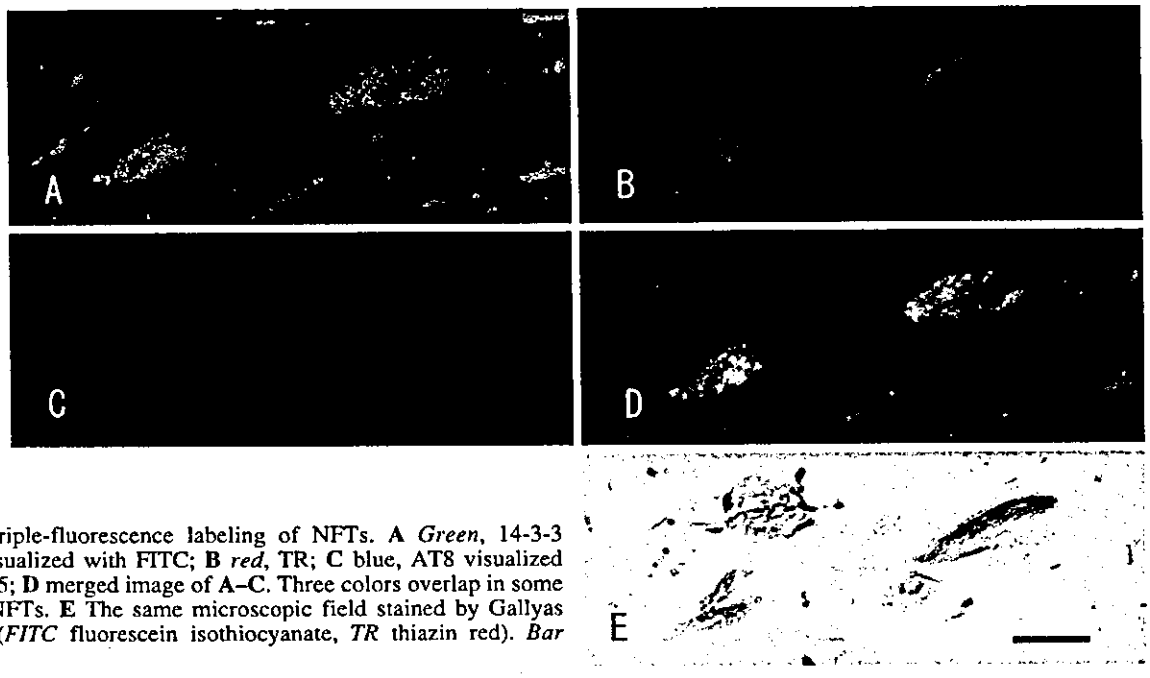

Fig. 6 Triple-fluorescence labeling of NFTs. **A** *Green*, 14-3-3 COM visualized with FITC; **B** *red*, TR; **C** blue, AT8 visualized with Cy-5; **D** merged image of **A**–**C**. Three colors overlap in some part of NFTs. **E** The same microscopic field stained by Gallyas method (*FITC* fluorescein isothiocyanate, *TR* thiazin red). *Bar* 25 μm

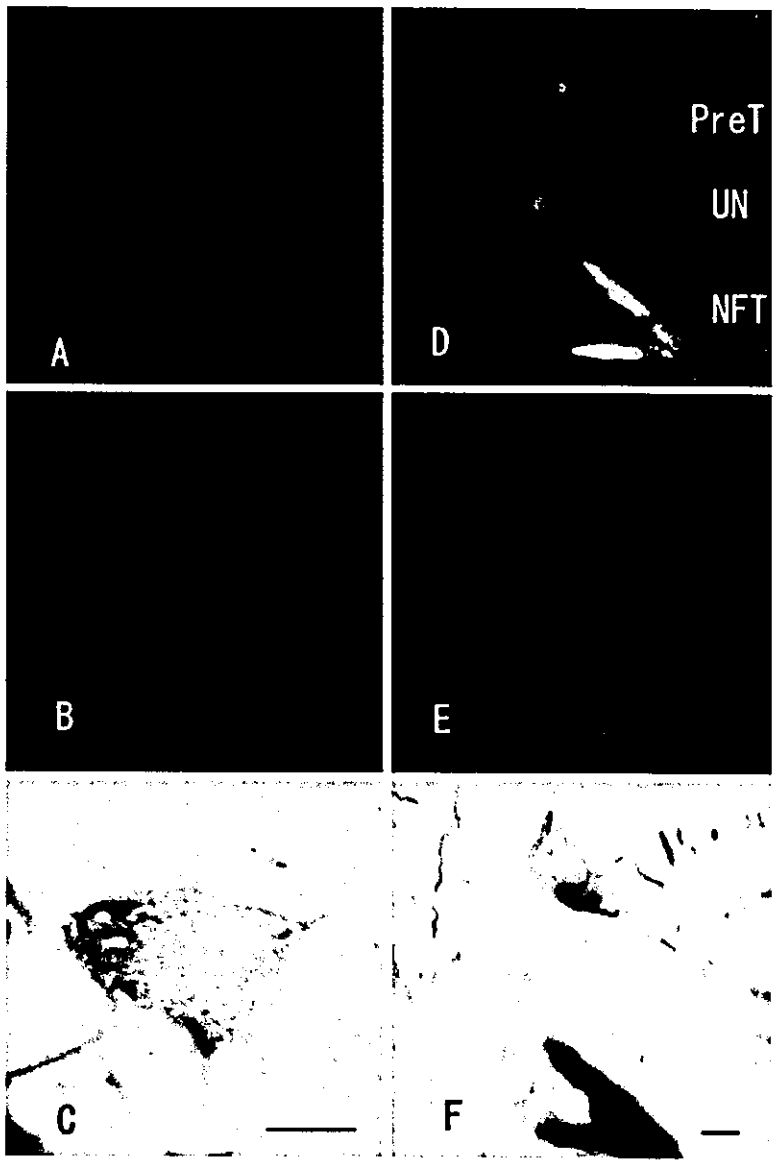

Fig. 7 A Triple-fluorescence labeling of a pretangle neuron. Merged image of 14-3-3 COM (*green*), TR (*red*) and AT8 (*blue*). B IR of 14-3-3 COM (*green*). C The same microscopic field stained by Gallyas method. IR of 14-3-3 proteins is not seen in this structure. D shows a pretangle neuron (*PreT*), an unaffected neuron (*UN*), and an NFT (merged image). This pretangle neuron only has fine granules immunolabeled by anti-14-3-3 COM antibody, which is similarly found in unaffected neuron. E IR of 14-3-3 COM (*green*). F The same microscopic field stained by Gallyas method. *Bars* 10 μm

Table 1 Immunoreactivity of hippocampus section by anti-14–3-3 proteins (*AD* Alzheimer's disease, *Control* elderly control subject, *NFTs* neurofibrillary tangles, *I-* intracellular, *E-* extracellular, *N-Th* neuropil threads)

Antibodies	AD			Control
	NFTs	N-Th	Others	
14–3-3 (common)	+++ I-NFTs, E-NFTs	+	Neuronal somata and processes	Neuronal somata and processes
Zeta	+++	+	Neuronal somata and processes	Neuronal somata and processes
Beta, gamma	+	±	Neuronal somata and processes	Neuronal somata and processes
Sigma	+	±	Granule cells in dentate gyrus	Granule cells in dentate gyrus
Epsilon	+	±	Neuropil and glial cells	Neuropil

mation or in functions related to neither tau deposition nor NFT formation. Indeed, NFT is not the only structure that contains 14-3-3 epitopes. For example, recent studies reported that GCIs in multiple system atrophy [18, 19] or Lewy bodies [17] are also rich in 14-3-3 epitopes. We do not yet know whether these cytoplasmic inclusions, more or less fibrillar in nature, share a common pathological cascade that involves 14-3-3 protein. Apart from these fibrillary inclusions, 14-3-3-like IR was also noted in the cytoplasm of neurons even in the presence of NFT. Because the presence of NFT did not influence the apparent intensity of this cytoplasmic 14-3-3-like IR, 14-3-3 protein may also be involved in processes not directly related to formation of fibril or inclusions.

In the present study, we used a panel of antibodies specific for each isoforms of 14-3-3 proteins (Table 1), since

there are few immunohistochemical studies using isoform-specific antibody in human brains. In control brains, beta, gamma, and zeta isoform-specific antibody showed findings almost similar to those obtained with the 14-3-3 COM antibody. Among them, it was the zeta isoform that immunolabeled many NFTs. This suggests that the zeta isoform is the major isoform deposited in NFT with fibrillary structure.

In contrast, immunolabeling of granule cells in the hippocampal dentate gyrus with the anti-sigma isoform antibody was enhanced in AD brains. This group of neurons are now attracting particular attention for their potential of neurogenesis [2, 16]. Moreover, peculiar tau-immunoreactive inclusions [24] were frequently found in these neurons in Pick body disease [35] or frontotemporal dementia linked to chromosome 17 [13]. Behaviors of these neurons may be distinct from what we observed on pyramidal neurons in hippocampus or cerebral cortex. If 14-3-3 proteins are involved in degenerative or regenerative processes, difference in expression of 14-3-3 protein isoforms may be linked to regional difference in these processes. This hypothesis, however, awaits confirmation.

Baxter et al. [4] reported that IR of the epsilon isoform was found in the gray matter of murine brain. Our results on human brain tissue were in agreement with theirs and are compatible with the hypothesis that epsilon isoform is closely associated synapses [4].

Although association of 14-3-3 epitopes has been described in a variety of fibrillary structures and inclusions [10, 17, 18, 19], there are some fibrillary deposits, for example senile plaques of AD, that apparently lack 14-3-3-like IR, as we confirmed in this study [27]. These indicate that fibrillary structures are not necessarily associated with 14-3-3-like IR. Moreover, it is interesting that some prion protein (PrP) deposits in Creutzfeldt-Jakob disease exhibit 14-3-3-like IR, while those in Gerstmann-Sträussler-Scheinker syndrome lack 14-3-3-like IR [27]. This contrast implies that conformational difference of the PrP, possibly explaining different morphologies of PrP plaques, is related to deposition of 14-3-3 protein. However, it remains to be clarified whether deposition of 14-3-3 is a secondary event dependent on preformed conformation or whether the deposition of 14-3-3 protein alters the conformation of other molecules to form deposits or inclusions.

The present study demonstrated that expression of 14-3-3 protein was highly variable and dependent on their isoforms, regions and cell types. Because each isoform has different functions under different conditions [4, 8, 10, 21, 27, 36], quantitative changes of 14-3-3 proteins in AD brains reported by Fountoulakis et al. [8] would be duly interpreted if data on cellular localization and regional difference are provided. Molecular, as well as topographical, dissection of 14-3-3 protein and its isoforms in relation to normal and pathological functions and structures will provide us with improved understanding of this molecule.

Acknowledgement This work is supported in part by grants for Sumitimo Welfare Foundation.

References

1. Agarwal-Mawal A, Qureshi HY, Cafferty PW, Yuan Z, Han D, Lin R, Paudel HK (2003) 14-3-3 connects glycogen synthase kinase-3β to tau within a brain microtubule-associated tau phosphorylation complex. J Biol Chem 278:12722–12728
2. Alyoman J, Das GD (1965) Autoradiographic and histological evidence of postnatal hippocampal neurogenesis in rats. J Comp Neurol 124:319–336
3. Aoki K, Uchihara T, Sanjo N, Nakamura A, Ikeda K, Tsuchiya K, Wakayama Y (2003) Increased expression of neuronal apolipoprptein E in human brain with cerebral infarction. Stroke 34:875–880
4. Baxter HC, Liu WG, Forster JL (2002) Immunolocalisation of 14-3-3 isoforms in normal and scrapie-infected murine brain. Neuroscience 109:5–14
5. Berg D, Holzmann C, Riess O (2003) 14-3-3 proteins in the nervous system. Nat Rev Neurosci 4:752–762
6. Boston PF, Jackspn P, Thompson RJ (1982) Human 14-3-3 protein: radioimmunoassay, tissue distribution, and cerebrospinal fluid levels in patients with neurological disorders. J Neurochem 38:1475–1482
7. Braak H, Braak A (1991) Neuropathological stageing of Alzfeimer-related changes. Acta Neuropathol 82:239–259
8. Fountoulakis M, Cairns N, Lubec G (1999) Increased levels of 14-3-3 gamma and epsilon proteins in brain of patients with Alzheimer's disease and Down syndrome. J Neural Transm 57: 323–335
9. Fu H, Subramanian RR, Masters SC (2000) 14-3-3 protains: structur, function, and regulation. Annu Rev Pharmacol Toxicol 40:617–647
10. Hashiguchi M, Sobue K, Paude HP (2000) 14-3-3 ζ is an effector of tau protein phosphorylation. J Biol Chem. 275: 25247–25254
11. Hsich G, Kenney K, Gibbs CJ, Lee KH, Harrington MG (1996) The 14-3-3 protain in cerebrospinal fluid as a maker for transmissible spongiform encephalopathy. N Engl J Med 335:924–930
12. Ichihara T, Isobe T, Okuyama T, Yamauchi T, Fujisawa H (1987) Brain 14-3-3 protein is an activator protein that activates tryptophan 5-monooxygenase and tyrosine 3-monooxygenase in the presence of Ca^{2+}, calmodulin-dependent protein kinase II. FEBS Lett 219:79–82
13. Iizima M, Tabira T, Poorkaj P, Schellenberg GD, Trojanowski JQ, Lee VM, Schmidt ML, Takahiashi K, Nabika T, Matsumoto T, Yamashita Y, Yoshioka S, Ishino H (1999) A distinct familial presenil dementia with a novel missense mutation in the tau gene. Neuroreport 25:497–501
14. Jones DH, Ley S, Aiken A (1995) Isoforms of 14-3-3 protein can form homo- and heterodimers in vitro: implications for function as adaptor proteins. FEBS Lett 368:55–58
15. Jones DH, Martin H, Madrazo J, Robinson KA, Nielson P, Roseboom PH, Patel Y, Howell SA, Aitken A (1995) Expression and structural analysis of 14-3-3 proteins. J Mol Biol 245:375–384
16. Kaplan MS, Bell DH (1984) Mitotic neuroblasts in the 9-day-old and 11-month-old rodent hippocampus. J Neurosci 4:1429–1441
17. Kawamoto Y, Akiguchi I, Nakamura S, Honjyo Y, Shibasaki H, Budka H (2002) 14-3-3 proteins in Lewy bodies in Parkinson disease and diffuse Lewy body disease brain. J Neuropathol Exp Neurol 61:245–253
18. Kawamoto Y, Akiguchi I, Nakamura S, Budka H (2002) Accumulation of 14-3-3 proteins in glial cytoplasmic inclusions in multiple system atrophy. Ann Neueol 52:722–731
19. Komori T Ishizawa K Arai N Hirose T Mizutani T Oda M (2003) Immunoexpression of 14-3-3 proteins in glial cytoplasmic inclusions of multiple system atrophy. Acta Neuropathol 103:66–70

20. Layfield R, Fergusson J, Aitken A, Lowe J, Landon L (1996) Neurofibrillary tangles of Alzheimer's desease brain contain 14-3-3 protain. Neurosci Lett 209:57–60
21. Martin H, Rostas J, Patel Y, Aitken A (1994)Subcellular localisation of 14-3-3 isoforms in rat brain using specific antibodies. J Neurochem 63:2259–2265
22. Mercken M, Vandermeeren M, Lubke U, Six J, Boons J, Van de Voorde A, Martin J-J, Gheuens J (1992) Monoclonal antibodies with selective specificity for Alzheimer tau are direcred against phosphatase-sensitive epitope. Acta Neuropathol 84: 265–272
23. Moore BW, Perez VJ (1967) In: Carlson FD (ed) Physiological and biochemical aspects of nervous integration. Prentice-Hall, New Jersey, pp 343–359
24. Murayama S, Nukina N, Ihara Y, Nakazato Y, Ishida Y, Takanashi R (1985) Immunocytochemistry of Pick's argentophilic bodies: evidence for the involvement of high molecular weight microtubule-associated proteins (HMWP) before the appearance of tubulin (in Japanese). Rinsho Shinkeigaku 25: 80–87
25. Muslin AJ, Tanner JW, Allen PM, Shaw AS (1996) Interaction of 14-3-3 with signaling proteins is mediated by the recognition of phosphoserine. Cell 84:889–897
26. Resch JF, Lehr GS, Wischik CM (1991) Design and synthesis of a potential affinity cleaving reagent for beta-pleated sheet protein structures. Bioorg Med Chem Lett 1:519–522
27. Richard M, Biacabe A-G, Streichnberger N, Ironside JW, Mohr M, Kopp Nicolas, Perret-Liauded A (2003) Immunohistochemical localization of 14-3-3ζprotein in amyloid plaques in human spongiform encephalopathies. Acta Neuropathol 105:296–302
28. Rosenquist M (2003) 14-3-3 proteins in apoptpsis. Braz J Med Biol Res 36:403–408
29. Satoh J, Kurohara K, Yukitake M, Kroda Y (1999) The 14-3-3 protain detectable in the cerebraospinal fluid of patients with prion-unrelated neurological diseases is expressed constitutively in neuronal and glial cells in culture. Eur Neurol 41: 216–225
30. Skoulakis EMC, Davis RL (1998) 14-3-3 protains in neuronal development and function. Mol Neurobiol 16:269–284
31. Tzivion G, Avruch J (2001) 14-3-3 proteins: active cofactors in cellular regulation by serine/threonine phosphorylation. J Biol Chem 14:3061–3064
32. Uchihara T, Nakamura A, Yamazaki M, Mori O (2000) Tau-positive neurons in corticobasal degeneration and Alzheimer disease-distinction by thiazin red and silver impregnations. Acta Neuropathol 100:385–389
33. Uchihara T, Nakamura A, Yamazaki M, Mori O (2001) Evolution from pretangle neurons to neurofibrillary tangles monitored by thiazin red combined with Gallyas method and double immunofluorescence. Acta Neuropathol 101:535–539
34. Uchihara T, Nakamura A, Yamazaki M, Mori O, Ikeda K, Tsuchiya K (2001) Different conformation of neuronal tau deposits distinguished by double immunofluorescence with AT8 and thiazin red and combined with Gallyas method. Acta Neuropathol 102:462–466
35. Uchihara T, Ikeda K, Tsuchiya K (2003) Pick body disease and Pick syndrome. Neuropathology 23:318-326
36. Wakabayashi H, Yano M, Tachikawa N, Oka S, Maeda M, Kido H (2001) Increased concentration of 14-3-3 epsilon, gamma, and zeta isofrms in cerebrospinal fluid of AIDS patients with neuronal destruction. Clin Chim Acta 312:97–105
37. Zha J, Harada H, Yang E, Jockel J, Korsmeyer SJ (1996) Serine phosphorylation of death agonist BAD in response to survival factor results in binding to 14-3-3 not BCL-X(L). Cell 87:619–692

Available online at www.sciencedirect.com
SCIENCE DIRECT
Neuroscience Letters 371 (2004) 215–219
Neuroscience Letters
www.elsevier.com/locate/neulet

Immunolocalization of 14-3-3 isoforms in brains with Pick body disease

Takahiko Umahara[a,b,*], Toshiki Uchihara[b], Kuniaki Tsuchiya[c], Ayako Nakamura[b], Kenji Ikeda[d], Toshihiko Iwamoto[a], Masaru Takasaki[a]

[a] *Department of Geriatrics, Tokyo Medical University, 6-7-1 Nishi-Shinjyuku, Shinjyuku-ku, Tokyo 160-0023, Japan*
[b] *Department of Neuropathology, Tokyo Metropolitan Institute for Neuroscience, 2-6 Musashi-dai, Fuchu, Tokyo 183-8526, Japan*
[c] *Department of Laboratory Medicine and Pathology, Tokyo Metropolitan Matsuzawa Hospital, 2-1-1 Kamikitazawa, Setagaya-ku, Tokyo 156-0057, Japan*
[d] *Department of Psychogeriatrics, Tokyo Institute of Psychiatry, 2-1-8 Kamikitazawa, Setagaya-ku, Tokyo 156-0057, Japan*

Received 15 December 2003; received in revised form 23 August 2004; accepted 30 August 2004

Abstract

Immunolocalization of 14-3-3 protein isoforms in relation to Pick bodies in Pick body disease (PBD) brains was investigated. Weakly granular immunoreactivity of 14-3-3 proteins was found in neurons in control subjects and in Pick body disease brains. In addition to this granular immunoreactivity, many Pick bodies were immunopositive for 14-3-3 proteins as confirmed with double-immunofluorescence with an anti-PHF tau (AT8) and anti-14-3-3 that recognizes all its isoforms (common). When probed with isoform-specific antibodies, Pick bodies were positive for beta, gamma, epsilon, eta, tau, and zeta isoform and exhibited immunostaining pattern similar to that observed with the anti-14-3-3 proteins (common). In addition, immunoreactivity of sigma isoform, so far considered to be exclusively extraneuronal, was unexpectedly found in Pick bodies, normal hippocampal neurons and brain homogenate from age-matched controls. Although localization of 14-3-3 proteins in Pick bodies suggests their involvement in Pick body formation, their role may be variable dependent on the isoforms differently expressed in different area in the brain.

Keywords: 14-3-3 proteins; Sigma isoform; Pick body; Pick body disease; Tau protein; Granule cells of the dentate gyrus

14-3-3 proteins are a family of highly conserved molecule of 30 kDa [5]. The proteins are mainly localized to the synapses and neuronal cytoplasm. Although they are known as adaptor proteins, which bind to the phosphoserine-containing motifs of the target protein, they are now endowed with a growing series of potential functions and pathological relevance [3,5,8,13].

Elevated 14-3-3 proteins in the cerebrospinal fluid are one of the potential indicators of transmissible spongiform encephalopathy [7]. The proteins regulate intercellular signal transduction by modulating phosphorylatin of the target proteins [3,5,8], and control apoptosis induced by BAD [13,18]. They are colocalized to a variety of deposits characteristic for some neurodegenerative processes, such as Lewy bodies (LBs) [10] or glial cytoplasmic inclusions (GCIs) [9,11] both consist of α-synuclein that shares structural homology with 14-3-3 proteins, and neurofibrillary tangles (NFTs) in Alzheimer's disease (AD) brains [12,16]. This raises the possibility that 14-3-3 proteins play some indispensable roles during formation of these deposits regardless of the diagnosis and prompted us to examine Pick bodies, another example of a disease-specific deposits. Seven isoforms (β: beta; γ: gamma; ε: epsilon; ζ: zeta; η: eta; τ: tau; and σ: sigma) of the protein have been so far identified in mammals [5]. However, physiological functions or pathological relevance of each isoform are yet to be clarified. We then decided to undertake an immunohistochemical study on a series of brains with Pick body disease (PBD) [15] or Pick's disease with Pick bodies [14] with

* Corresponding author. Tel.: +81 3 3342 6111; fax: +81 3 3342 2305.
E-mail address: takahiko@tokyo-med.ac.jp (T. Umahara).

0304-3940/$ – see front matter © 2004 Elsevier Ireland Ltd. All rights reserved.
doi:10.1016/j.neulet.2004.08.079

a panel of antibodies specific for each isoform known to date.

In this study, we used following primary antibodies (Immuno-Biological Laboratories, Gunma, Japan), raised in rabbit against human 14-3-3 protein (1:2000, anti-14-3-3 COM raised against common sequence KDSTLIMQLLRDNLT shared by all isoforms) or its each isoform (anti-beta MTMDKSELVQ: 1:500, anti-gamma QQDDDGGEGNN: 1:200, anti-epsilon EQNKEALQDVEDENG: 1:500, anti-zeta MDKNELVQK: 1:200, and anti-sigma (C) EEGGEAPQEPQS: 1:300, anti-eta MGDREQLLQR, isforms) and used anti-14-3-3 tau isoform monoclonal antibody (raised against recombinant human 14-3-3 tau) [17]. Specificity of six of these antibodies (14-3-3 COM, beta, gamma, epsilon, zeta, and sigma isoforms) was established previously on Western blot [16,17] and absorption studies (14-3-3 COM and zeta isoform) [16]. Other antibodies were tested for their specificity for each isoform on Western blot (sigma isoform) and by absorption of immunolabeling upon coincubation with the antigen peptide, as described below. Briefly, control brains [2] were homogenized in an ice-cooled fixative 10% trichloroacetic acid. Each pellet was solubulized by sonication in a sample buffer containing 9 mol/L urea, 2% Triton X, and 5% 2-mercaptoethanol. Then one-fifth volume of 10% lithium dodecyl sulfate solution and approximately 2 μL of 1 mol/L Tris solution were added to sample buffer, and the samples were sonicated again.

Lysates containing equal amounts of protein (20 μg) were subjected to 10% sodium dodecyl sulfate-poly-acrylamide gel electrophoresis. Transferred protein were probed with the anti 14-3-3 sigma isoform (1:200) antibody and visualized with the use of an enhanced chemiluminescence system (Amersham, Arlington Heights, IL).

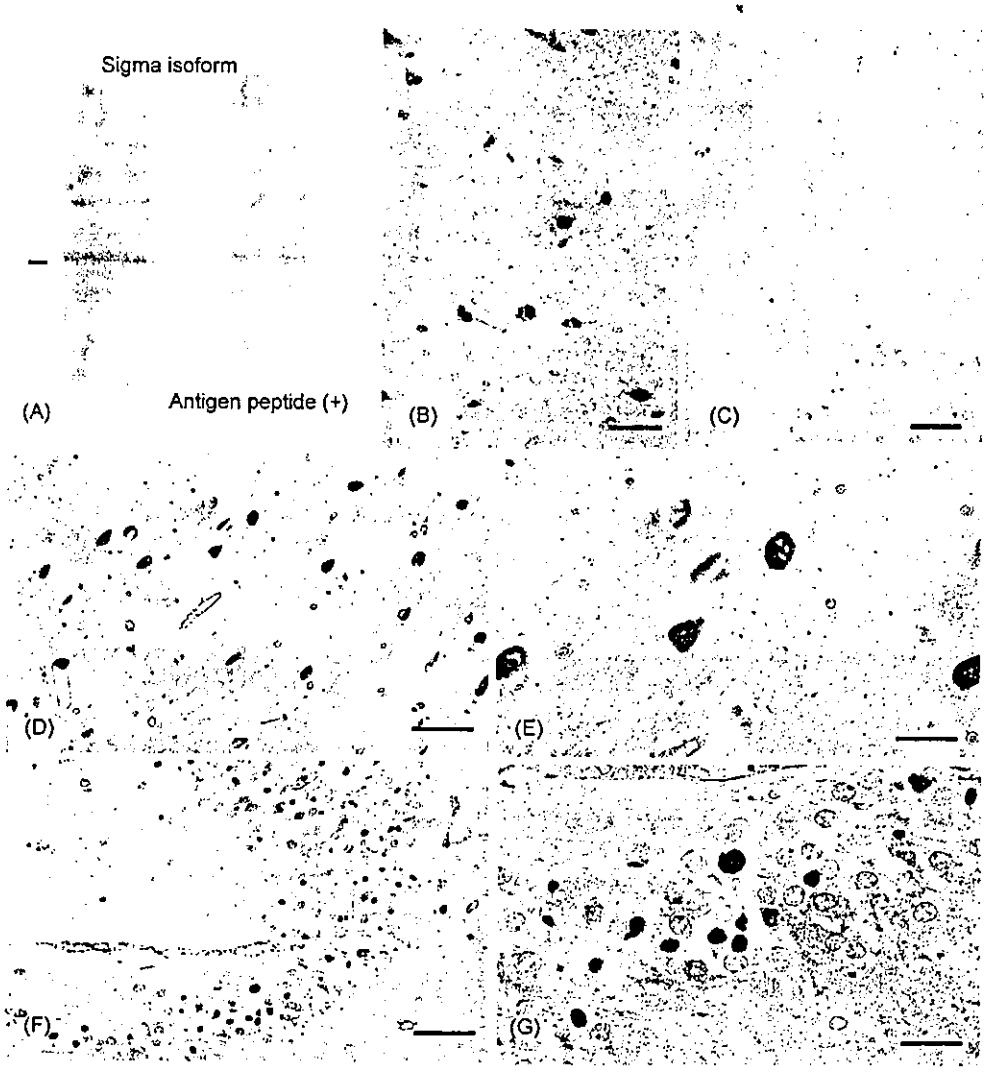

Fig. 1. Pick bodies probed with anti-14-3-3 antibodies in hippocampal sections from Pick body disease brains. (A) Western blot of extracts from human control subject brains probed with the anti-sigma isoform antibody. A faint band at approximately 30 kDa is detectable (left panel), which is abolished when coincubated with the antigen peptide (right panel). Bar: 30 kDa. (B) 14-3-3 common (COM)-immunoreactive Pick bodies. (C) This immunoreactivity was abolished when the antigen peptide was added to the solution containing the primary antibody. (D–G) Pick bodies in hippocampal pyramidal neurons (D and F) and in granule cells in the dentate gyrus (F and G) were clearly immunolabeled by 14-3-3 COM. Bar (B–D and F) 50 μm; (E and G) 20 μm.

In our previous report, probing human brain extracts with the anti-14-3-3 COM and zeta isoform demonstrated a major band at approximately 30 kDa in control and AD brain [16]. In this study, that of the anti-sigma isoform similarly demonstrated a faint band at approximately 30 kDa in the brain homogenate. This immunopositive band was abolished when the antigenic peptide was added to the solution containing the primary antibody (Fig. 1A).

With these isoform-specific antibodies, immunolocalization of each epitope was examined on hippocampal specimens obtained from four elderly control subjects (67–85 years old) and from four patients with PBD (56–83 years old). Five micronmeter-thick sections were obtained from formalin-fixed, paraffin-embedded blocks. After being autoclaved in a citrate buffer at 120 °C for 20 min, they were treated with 1% hydrogen peroxide for 30 min. Sections were incubated with one of the primary antibodies for 2 days.

They were then incubated with the appropriate biotinylated secondary antibody for 2 h at a dilution of 1:1000. After incubation with the avidin–biotin-peroxidase complex (1:1000, ABC Elite, Vector Laboratories, Burlingame, CA) for 1 h, peroxidase labeling was visualized with 0.03% 3,3-diaminobenzidine, 0.6% nickel ammonium sulfate, 0.05 M imidazole and 0.00015% hydrogen peroxide. A deep purple immunoreaction product appeared after 15–20 min.

Immunolocalization of 14-3-3 epitopes and their relation to Pick body were further investigated with double-fluorolabeling with the anti 14-3-3 COM antibody (1:1600) and an anti-PHF tau monoclonal antibody (1:1000, AT8, Innogenetics, Zwijndrecht, Belgium) that recognizes phosphatase-senseitive serine 199 and 202 epitopes of tau protein but does not cross-react with normal tau proteins. 14-3-3 epitopes were probed with an anti-rabbit IgG conjugated with horseradish peroxidase (1:500, Pierce, Rockford, IL) followed by amplification with biotinylated tyarmide (1:1000), and was finally visualized with streptavidin-coupled FTIC (1:200, Vector Laboratories, Burlingame, CA). The PHF-tau epitope was simultaneously visualized with anti-mouse IgG (Fc γ-fragment specific) coupled with Rhodamin Red (1:200, Jackson ImmunoReseach, West Grove, PA).

Sections were observed under an epifluorescence microscope combined with laser confocal system (TCS-SP, Leica, Heidelberg, Germany). FITC (emission peak: 518 nm) was detected through a 500–540 nm light path. Emission from Rhodamin Red (emission peak: 590 nm) was detected through a 590–620 nm light path. Each of the fluorescence signals was considered positive when it was more intense than the autofluorescence of lipofuscin granules.

In hippocampal sections from elderly control subjects, weak granular 14-3-3-like IR (anti-14-3-3 COM) was observed in neuronal cytoplasm and processes of some hippocampal pyramidal neurons in all cases.

In the hippocampus of PBD brains, the anti-14-3-3 COM antibody immunolabeled some neuronal cytoplasm and many Pick bodies (Fig. 1B). This immunoreactivity was abolished when the antigen peptide (14-3-3 COM) was added to the solution containing the primary antibody (Fig. 1C).

Pick bodies in hippocampal pyramidal neurons (Fig. 1D and E) and in granule cells in the dentate gyrus (Fig. 1F and G) were clearly immunolabeled by this anti-14-3-3 COM antibody.

Hyppocampal neurons were stained with the anti-sigma antibody both in control (Fig. 2A) and PBD brains (Fig. 2B and C). Although granule cells in the dentate gyrus, where

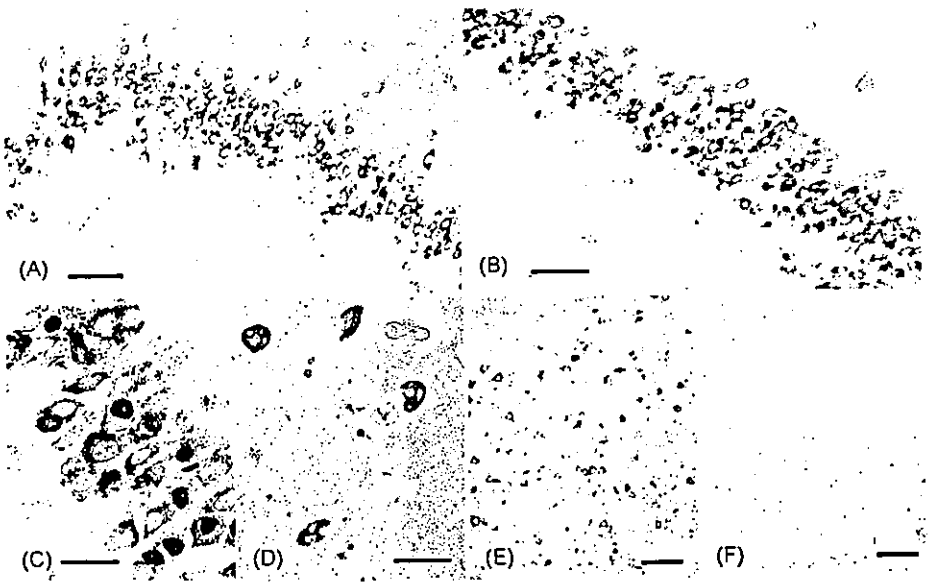

Fig. 2. (A–C) Granule cells in the dentate gyrus of control section (A) and Pick body disease brain (B and C) were immunolabeled for the sigma isoform. Numerous Pick bodies immunopositive for sigma isoform. (D) Anti-beta isoform antibody immunolabels Pick bodies, some of which contain unstained regions inside them. (E and F) Hippocampal neurons were immunolabeled for the sigma isoform (E). This immunoreactivity was abolished when the antigen peptide was added to the solution containing the primary antibody (F). Bar (A, B, E, and F) 50 μm; (C and D) 20 μm.

frequent appearance of Pick bodies is the rule, this sigma isoform-like immunoreactivity was far more intense in Pick bodies in these granule cells (Fig. 2 B and C) than those in other cortical areas. Neuropil of the cerebral cortex was homogeneously stained with the anti-epsilon antibody (data not shown). When probed with either anti-beta, anti-eta, anti-gamma, anti-tau, or anti-zeta isoform-specific antibody against 14-3-3, Pick bodies in PBD brains, as well as neurons in controls, exhibited immunostaining pattern similar to that observed with the anti-14-3-3 COM. Immunolabeling for these isoforms was less intense than that for 14-3-3 COM (data not shown). 14-3-3-like immunoreactivity in Pick bodies was not homogenous and some unstained areas were sometimes detected in Pick bodies, as shown with the anti-beta isoform-specific (Fig. 2D). Those isoform-related immunoreactivities were also abolished when each isoform antigen peptide was added to the solution containing the primary antibody (Sigma isoform-like immunoreactivity in hippocampal neurons in control brains and its effacement upon coincubation with the isoform-specific peptide, as shown in Fig. 2E and F, respectively).

Fig. 3 shows immunolocalization of 14-3-3 proteins (FITC: green) and PHF-tau (AT8-Rhodamin Red: red) in the hippocampus. The 14-3-3 epitope was colocalized to around 80% Pick bodies immunolabeled for PHF-tau.

The anti-14-3-3 antibodies used in the present study probed a single band of 30 kDa that corresponds to an expected molecular weight of 14-3-3 proteins on Western blot [16]. Immunohistochemical labeling, as well as the immunoreactive bands on Western blot [16], was abolished when the primary antibody (14-3-3 COM, zeta isoform [16] or sigma isoform) was coincubated with the corresponding antigen peptide (Fig. 1B and C for 14-3-3 COM, and Fig. 2A–D for 14-3-3 sigma).

It has been reported that 14-3-3 proteins, potentially binds to the microtubule-binding region of tau, regardless of phosphorylation state of tau [6]. In addition, it potentially stimulates phosphorylation of recombinant tau by activating protein kinase A and neuronal cdc2-like kinase. Another report [1] demonstrated that zeta isoform dimer simultaneously binds and bridges tau and GSK3β and stimulates GSK3β-catalyzed tau phosphorylation. These lines of evidence suggest that possible participation of 14-3-3 proteins in phosphorylation of tau. Indeed, presence of 14-3-3 epitope in neurofibrillary tangles in Alzheimer disease brains [12,16] is compatible with this interpretation. The present study demonstrated immunolocalization of 14-3-3 proteins in Pick bodies, another deposits with phosphorylated tau. Although we do not yet know whether the mechanism of tau phosphorylation in PBD is similar to that in AD, immunolocalization of GSK 3β in Pick bodies [4] suggest that this enzyme has potential relevance to tau phosphoryaltion both in AD and PBD. It is, then, possible that 14-3-3 proteins, potentially related to activation of GSK 3β, may also play some role during tau phosphorylation both in AD and Pick body disease. This was further confirmed by multilabeling method with PHF-tau.

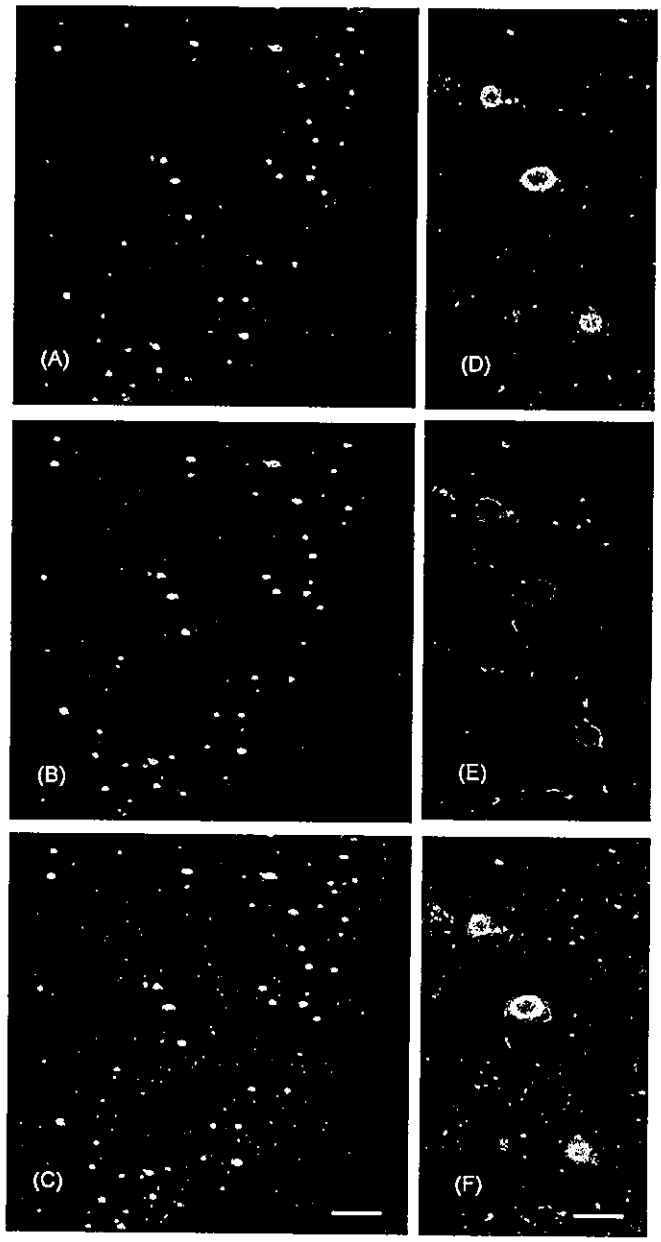

Fig. 3. Double-fluorescence labeling of Pick bodies. (A and D) Green, 14-3-3 COM visualized with FITC. (B and E) Red, phosphorylated tau (AT8) epitope visualized with Rhodamin Red. (C and F) Merged image of (A and B) and (D and E) respectively. Most of the Pick bodies, immunoreactive to AT8 (red), are also positive for 14-3-3 COM (green). Bar (C) 50 μm and (F) 20 μm.

Possible participation of 14-3-3 protein in tau phosphorylation is, however, challenged because accumulation of this protein is not restricted to tau deposits but also has been reported in a variety of deposits such as glial or neuronal cytoplasmic inclusions of multiple system atrophy [9,11] or Lewy bodies [10]. 14-3-3 proteins may, therefore, play some different roles dependent of each process. One of the possibilities, however, may include that this protein is involved in a mechanism shared by the formation of protein deposits regardless of the molecular constituents of each deposit.